Youth-associated protein TIMP2 alters microglial state and function in the context of aging

Brittany M. Hemmer[1,2,3,4,5], Ana Catarina Ferreira[1,2,3,4], Sarah M. Philippi[1,2,3,4,5], Samuele F. Petridis[1,2,3,4], Annie Phan[1,2,3,4], Joseph M. Castellano[1,2,3,4]*

[1]Nash Family Department of Neuroscience, Friedman Brain Institute, Icahn School of Medicine at Mount Sinai, New York, NY, USA

[2]Ronald M. Loeb Center for Alzheimer's Disease, Icahn School of Medicine at Mount Sinai, New York, NY, USA

[3]Department of Neurology, Icahn School of Medicine at Mount Sinai, New York, NY, USA

[4]Black Family Stem Cell Institute, Icahn School of Medicine at Mount Sinai, New York, NY, USA

[5]Graduate School of Biomedical Sciences, Icahn School of Medicine at Mount Sinai, New York, NY, USA

*Correspondence:

Joseph Castellano, Ph.D.

Icahn School of Medicine at Mount Sinai

1425 Madison Avenue, Box 1065

Phone: 212-659-5913

E-mail: joseph.castellano@mssm.edu

Abstract

There is little understanding of how aging serves as the strongest risk factor for several neurogenerative diseases. Specific neural cell types, such as microglia, undergo age-related maladaptive changes, including increased inflammation, impaired debris clearance, and cellular senescence, yet specific mediators that regulate these processes remain unclear. The aged brain is rejuvenated by youth-associated plasma factors, including tissue inhibitor of metalloproteinases 2 (TIMP2), which we have shown acts on the extracellular matrix (ECM) to regulate synaptic plasticity. Given emerging roles for microglia in these processes, we examined the impact of TIMP2 on microglial function. We show that TIMP2 deletion exacerbates microglial phenotypes associated with aging, including transcriptomic changes in cell activation, increased microgliosis, and increased levels of stress and inflammatory proteins measured in the brain extracellular space by *in vivo* microdialysis. Deleting specific cellular pools of TIMP2 *in* vivo increased microglial activation and altered myelin phagocytosis. Treating aged mice with TIMP2 reversed several phenotypes observed in our deletion models, resulting in decreased microglial activation, reduced proportions of proinflammatory microglia, and enhanced phagocytosis of physiological substrates. Our results identify TIMP2 as a key modulator of age-associated microglia dysfunction. Harnessing its activity may mitigate detrimental effects of age-associated insults on microglia function.

Introduction

Aging is accompanied by progressive functional decline across multiple organ systems, but its impact on the brain is especially devastating given the dysfunction wrought across key cognitive domains and the increased risk it poses for several neurological disorders. These changes reflect cumulative cellular, molecular, and structural perturbations, including decreased generation of newborn neurons, loss of synaptic and myelin integrity, and microgliosis in vulnerable brain regions like the hippocampus. Understanding mechanisms that regulate aging in the

49 hippocampus is thus essential for identifying new strategies to preserve or restore function across
50 lifespan and to limit risk for neurological disease. Interestingly, the process of aging and AD pose
51 similar challenges to the brain's immune environment, including aberrant inflammation and
52 elevated exposure to lipid-rich debris from dying cells[1]. The role of microglia, the brain's innate
53 immune cells, in responding to aging-associated damage has emerged as a promising avenue
54 for investigation, galvanized by the identification of many myeloid-enriched genes associated with
55 AD risk in a series of GWAS over the past decade[2]. While specific states adopted by microglia
56 may initially be protective to limit pathology to surrounding brain tissue, chronic challenges and
57 exposure to debris may create maladaptive responses,[3-6] which manifests as phagocytic
58 ineptitude[7-10], production of inflammatory cytokines[11,12], and increased stress responses[6,13]. Thus,
59 there is a need to identify means to rejuvenate the response of these cells to aging-associated
60 challenges to provide a path for novel therapies that limit the impact of aging on neurological
61 disorders.
62
63 Modulating the systemic environment has emerged as a promising strategy to counteract age-
64 related decline in cellular function. Exposure to factors present within young blood rejuvenates
65 the aged brain[14,15], leading to increased synaptic plasticity[16-18] and dendritic spine integrity[17],
66 enhanced vascular remodeling[19], and improved learning and memory performance in aged
67 mice[16-18]. While much of this work has focused on the impact of blood-borne factors directly on
68 neurons or adult neuroblasts in the hippocampus, recent work has suggested that microglia can
69 take up labeled proteins originating in plasma[20,21], suggesting that they may be responsive to
70 blood-borne factors. Moreover, in response to treatment with plasma or a platelet factor that acts
71 on immune cells in the periphery, microglia appear to exhibit altered phagocytosis[21] and activation
72 state[18], respectively. Despite these intriguing findings, the field lacks detailed characterization of
73 how specific youth-associated factors affect microglial function and how such factors can be
74 harnessed to revitalize the aged brain.

75

76 We previously identified tissue inhibitor of metalloproteinases 2 (TIMP2) as a youth-associated
77 blood-borne factor that is capable of revitalizing hippocampal function in aged mice[16]. Levels of
78 TIMP2 are elevated in very young human and mouse plasma and rapidly decline into adulthood
79 and old age[16]. Interestingly, a recent study finds that those expressing *TIMP2* variants associated
80 with higher plasma protein levels exhibit higher cognitive performance in a cohort of aged
81 individuals[22]. Aged mice treated systemically with TIMP2 exhibit similar improvements as mice
82 treated with young plasma, including increased hippocampal plasticity and cognitive
83 improvements, likely as a result of direct TIMP2 action on CNS cells given its entry from blood
84 into brain[16]. While TIMP2 has many canonical and non-canonical targets[23,24], these studies
85 suggest that TIMP2 has myriad roles within the hippocampal microenvironment, and its role in
86 modulating innate immune function is understudied. We recently reported that TIMP2 plays a
87 critical role in the young hippocampus in regulating memory, synaptic integrity, and adult
88 neurogenesis through modulation of ECM homeostasis[25], processes that have been found to be
89 regulated by microglia[26,27]. Given the modulation by TIMP2 in processes linked to microglia
90 function and the rejuvenating capacity of TIMP2 in aging contexts, we sought to determine how
91 TIMP2 affects basic microglial function and whether systemic supplementation can restore
92 protective microglial activities that are lost with exposure to age-associated insults.

93

94 Here we show that loss of TIMP2 expression from a variety of sources (i.e., removal from global,
95 microglial, and neuronal sources) alters microglia by increasing activation, elevating their
96 inflammatory state, and shifting phagocytosis—all processes associated with aging. Restoring the
97 extrinsic pool of TIMP2 in aged mice through systemic TIMP2 treatment reversed these age-
98 associated phenotypes by reducing microgliosis and specific inflammatory microglial
99 subpopulations and by increasing phagocytosis of physiological substrates in the hippocampus.
100 Together our results demonstrate that the youth-associated protein TIMP2 plays a novel role in

101 modulating microglial function by shifting their responses to accommodate detrimental aging
102 pathologies in a protective fashion. This work firmly positions TIMP2 as a relevant therapeutic
103 target to limit aging pathology and highlights the need for further mechanistic investigation into
104 how systemic factors modulate innate immune function in the brain.
105
106 **Results**
107
108 **Early deletion of TIMP2 alters microglial state**
109 TIMP2 is expressed in cells of the periphery, contributing to high levels in the plasma[16], and also
110 hippocampal neurons within the CNS[25], with expression in both compartments declining with
111 age[16]. Interestingly, *Timp2* has been shown to be upregulated in subpopulations of microglia in
112 response to aging and AD pathology as part of a panel of genes termed the disease-associated
113 microglia (DAM) profile[28]. To explore its expression within microglia, we noted its enriched
114 transcript abundance within microglia in published transcriptomic atlases, including in *Tabula*
115 *Muris Senis*[29], and in the Allen Brain Cell scRNAseq and MERFISH Atlas[30], in which *Timp2* is
116 expressed at high levels in the brain, particularly in hippocampal microglia (**Supplementary Fig.**
117 **1a-c**). To begin to characterize whether microglia express TIMP2 at the protein level and how its
118 loss influences function at early stages, we isolated primary microglia from neonatal forebrain
119 from wild-type (WT) and TIMP2 knock-out (KO) mice (**Fig. 1a**) at an age when global TIMP2 levels
120 are high[16]. We find high levels of TIMP2 protein by both immunoblotting of primary microglia
121 lysates and immunocytochemistry (ICC), whereas TIMP2 was not detected in TIMP2 KO microglia
122 (**Fig. 1b-c**). We next sought to understand what pathways may be disrupted by its loss in microglia
123 by performing bulk RNA-sequencing on WT and KO primary microglia (**Fig. 1a**). As expected, KO
124 microglia lacked *Timp2* transcript (**Fig. 1d**), and we detected a number of differentially expressed
125 genes in KO microglia relative to WT (252 upregulated, 316 downregulated; **Supplementary Fig.**
126 **1d**). To gain insight into what pathways are perturbed in microglia by TIMP2 deletion, we

127 performed over-representation analyses for gene ontology (GO)[31] terms related to 'biological
128 processes' and 'cellular components'. Genes that were upregulated in KO microglia were
129 significantly enriched in terms for "cell activation involved in immune response" and "positive
130 regulation of cytokine production", among others (**Fig. 1e**). Downregulated DEGs in KO microglia
131 were significantly enriched in pathways related to "synapse" and "neurogenesis" (**Fig. 1e**). The
132 transcriptomic profile of KO microglia may reflect a more activated and perhaps inflammatory
133 state relative to WT microglia, potentially regulating their communication with neurons and ability
134 to promote plasticity, as suggested in perturbed pathways identified by Ingenuity Pathway
135 Analysis (IPA) (**Supplementary Fig. 1e)**.

136 Given TIMP2's potential relationship with activation state, we stained cultures of primary
137 microglia isolated from adult mice and found that the majority of TIMP2-expressing cells co-
138 express CD68, a lysosomal-associated protein found enriched in myeloid cells (**Fig. 1f-g),**
139 pointing to a potential role for TIMP2 in regulating lysosomal function or activation state. While
140 not all microglia were found to express TIMP2, a sizeable fraction of microglia expressing CD68
141 co-expressed TIMP2 (**Supplementary Fig. 1f-h**).

142

143 **TIMP2 deletion increases hippocampal microgliosis and extracellular inflammatory**
144 **proteins**

145 To evaluate the extent to which the putative pathways identified in our profiling of KO and WT
146 microglia may reflect microglial phenotypes *in vivo* consistent with elevated activation state, we
147 next sought to characterize microglial activation in KO and WT dentate gyrus of the adult
148 hippocampus, a relevant region based on previous work demonstrating its role in regulating
149 plasticity processes[16,25]. Using confocal microscopy, we evaluated microglia by co-staining for
150 microglia marker IBA1 and activation marker CD68, which we previously found co-expressed with
151 TIMP2 in primary microglia (**Fig. 1f-g**). As early as 3-4 months of age, KO mice exhibited a trend
152 towards an increase in the percentage of dentate gyrus (DG) covered by IBA1 staining relative to

153 WT (**Fig. 2a-b**), perhaps reflecting early changes in microglial morphology. While levels were
154 modestly low given the early age, we detected significantly more microglia co-expressing CD68
155 in KO dentate gyrus compared to that from WT mice (**Fig. 2a,c**), as well as higher percentage
156 area covered by CD68 (**Supplementary Fig. 2a-b)**, indicating increased microgliosis. TIMP2
157 deletion did not affect the total number of microglia (**Supplementary Fig. 2a,c)**.

158 We next examined if these changes persist or worsen at a later age, given the well-
159 established age-dependent microgliosis that occurs in the hippocampus[32]. At 6-7 months of age,
160 we found that while the total number of microglia was not affected by TIMP2 deletion
161 (**Supplementary Fig. 2d-e)**, the percentage of DG area occupied by IBA1 immunoreactivity was
162 significantly higher in the DG of TIMP2 KO compared to WT DG (**Fig. 2d-e**). To further
163 characterize this change, we performed a morphology analysis that broadly categorizes microglia
164 as "ramified", "activated", or "ameboid" based on their circularity using an established method
165 (**Supplementary Fig. 2f**)[33-36]. Our morphology analysis revealed an increased number of
166 morphologically "activated" microglia in the DG of KO mice relative to WT, with no change in the
167 number of "ramified" or "ameboid" microglia (**Supplementary Fig. 2g-j**). At this age, we also
168 detected a robust elevation in the number of $IBA1^{+}CD68^{+}$ cells in the DG of KO mice compared
169 to WT, reflecting the increased state of activation (**Fig. 2d,f**).

170 In inflammatory contexts, it is well-established that microglia release cytokines and other
171 factors into the extracellular space, affecting the cellular microenvironment of the brain. Given the
172 increased microgliosis found in KO hippocampus, we next sought to assess whether deletion of
173 TIMP2 alters the extracellular milieu. Conventional tissue-based assessment of cytokines and
174 chemokines do not accurately reflect the composition of the brain interstitial fluid (ISF) given loss
175 of compartmental barriers and effects of extraction methods on sensitivity, and this approach is
176 limited to postmortem sampling, which may not sufficiently capture the dynamics of immune
177 changes. To circumvent these issues, we employed high molecular-weight cut-off (HMWCO; 1-
178 MDa) *in vivo* microdialysis to sample the hippocampal ISF of awake and freely moving mice (**Fig.**

179 **2g**)[37,38]. This technique has not yet been extensively applied to measure brain immune proteins,
180 which are typically present in the brain ISF at very low levels. To establish this method's potential
181 to examine immune-related proteins in the brain ISF, we administered a single systemic injection
182 of lipopolysaccardine (LPS; 5 mg/kg), an established pro-inflammatory stimulus[39], as a proof-of-
183 concept approach in a 5XFAD model of amyloid pathology that should exhibit high baseline
184 cytokine and chemokine levels in the brain. Following microdialysis probe insertion into
185 hippocampus and a subsequent equilibration period to allow levels of ISF proteins stabilize, as
186 previously described[40,41], samples were collected over a baseline period before LPS treatment.
187 Samples were collected 10 hours following LPS and pre- and post-LPS period ISF samples were
188 quantified using an exploratory proximity extension assay (PEA)-based panel of cytokines,
189 chemokines, and related proteins (**Fig. 2h**). As shown in **Fig. 2i**, a number of expected pro-
190 inflammatory cytokines and chemokines were significantly elevated in the hippocampal ISF
191 following LPS treatment compared to the baseline period, including IL1β, CCL5, TNF, IL6, as well
192 as anti-inflammatory protein IL-10, which has been shown to be released by microglia following
193 LPS as a means to resolve the inflammatory response[42] (**Fig. 2i**). Having successfully dialyzed
194 and detected immune-related proteins using this method, we sought to assess the impact of
195 TIMP2 deletion on the hippocampal extracellular milieu. 2-3-month-old WT and KO mice were
196 subjected to the HMWCO *in vivo* microdialysis paradigm to sample hippocampal ISF during a
197 stable, steady state period of 24 hours for measurement of proteins in pooled ISF samples (**Fig.**
198 **2j**). Interestingly, deletion of TIMP2 increased a number of proteins associated with inflammation
199 in the hippocampal ISF (**Fig. 2k)**, including chemokine CCL20 that we had found to be elevated
200 following LPS stimulation (**Fig. 2i**), and EDA2R, a member of the tumor necrosis factor receptor
201 superfamily whose levels correlates with increased age[43]. EDA2R cytokine signaling contributes
202 to inflammation through activation of the NF-κB pathway. TIMP2 deletion also increased
203 hippocampal ISF levels of HGF, a pleiotropic cytokine that modulates the inflammatory response

204 through NF-κB signaling that is also elevated in CSF of AD subjects[44,45]. Several proteins known
205 to be upregulated under neurotoxic conditions as a means to limit damage were also found to be
206 upregulated in TIMP2 KO ISF, including EPO, GFRA1, TGFA[46,47], as was the lysosomal serine
207 protease TPP1 that is associated with phagocytic function[48,49]. As expected, we also found that
208 loss of TIMP2 increases hippocampal ISF levels of Matrilin-2 (MATN2), an extracellular matrix
209 (ECM) protein[25] that signals through TLR4 to induce proinflammatory genes in macrophages to
210 promote axonal damage[50]. Together, these changes in the hippocampal extracellular environment
211 may reflect a more pro-inflammatory, debris-rich environment relative to that in WT hippocampus.
212

213 **Microglial TIMP2 regulates activation state**

214 Our findings suggest that loss of TIMP2 alters microglial activation and contributes to an
215 inflammatory extracellular environment, yet it remains unclear whether these differences are
216 mediated by the pool of TIMP2 produced by microglia, consistent with its expression pattern
217 demonstrated in our previous experiments (**Fig. 1b-c**). To explore the contribution of microglial
218 sources of TIMP2 to the microglial phenotypes associated with global TIMP2 deletion, we used a
219 TIMP2$^{fl/fl}$ model we generated[25] and crossbred them with *Cx3cr1*$^{CreERT2/+}$ mice[51] to inducibly delete
220 TIMP2 in *Cx3cr1*-expressing cells (e.g., microglia). Using a previously established adult microglia
221 isolation paradigm[52] (**Fig. 3a**) that successfully yielded pure adult microglia in culture
222 (**Supplementary Fig. 3a-c)**, we first induced Cre-mediated recombination and then confirmed
223 efficient deletion of microglial TIMP2 (**Supplementary Fig. 3d-e**). To examine how TIMP2
224 deletion in microglia affects canonical activation marker expression, we imaged primary adult
225 microglia expressing CD68. Targeting microglial expression of TIMP2 significantly increased the
226 number of cells expressing CD68 (**Fig. 3b-c**). We also quantified the number of primary microglia
227 expressing senescent marker p16INK4a given the earlier pathway association in TIMP2 KO
228 neonatal microglia (**Supplementary Fig. 1h)**, which revealed a greater number of p16INK4a^{+}
229 microglia from *Cx3cr1*$^{CreERT2/+}$;*Timp2*$^{fl/fl}$ mice compared to that observed from *Timp2*$^{fl/fl}$ control

230 mice. (**Fig. 3d-e**). We next examined the number of IBA1^{+}CD68^{+} cells in the DG of 6-7 month-old
231 *Cx3cr1*$^{CreERT2/+}$;*Timp2*$^{fl/fl}$ mice or *Timp2*$^{fl/fl}$ control mice that had received tamoxifen (**Fig. 3f**). We
232 observed an increase in the extent of IBA1 staining covering the DG and an increase in the
233 number of activated microglia (IBA1^{+}CD68^{+}) (**Fig. 3f-h**). These findings suggest that removal of
234 the microglial pool of TIMP2 leads to microgliosis phenotypes that are consistent with those
235 observed in the setting of global TIMP2 deletion.
236

237 **Microglia contribute to external pools of TIMP2 and its removal modifies myelin**
238 **phagocytosis**

239 TIMP2 is present at high levels in the extracellular space of the hippocampus[25], likely reflecting
240 contributions from various sources, including from neurons and microglia. Our data show that
241 microglia express TIMP2 at both transcript and protein levels, yet it remains unclear whether
242 microglia release TIMP2, where it can potentially alter microglial response to pathological debris,
243 and whether targeting microglial TIMP2 affects associated phenotypes. To begin to explore these
244 questions, we isolated and cultured adult WT microglia to examine TIMP2 release into the media
245 across various timepoints in serum-free media, which was necessary given the high levels of
246 endogenous TIMP2 present in plasma/serum, especially at early life stages[16] (**Fig. 4a**).
247 Immunoblotting analysis on media from these cultures revealed that microglia release TIMP2 in
248 a time-dependent fashion (**Fig. 4b-c**). We then asked whether levels of TIMP2 released into the
249 media is modulated by exposure to various biological substrates (zymosan, 10 μg/mL; LPS, 100
250 ng/mL), including those commonly encountered within the brain (myelin, 10 μg/mL). 12 hours
251 following stimulation with these substrates, we measured TIMP2 levels in the conditioned media
252 by immunoblotting. While zymosan stimulation did not change TIMP2 levels in the media relative
253 to unstimulated conditions, LPS slightly increased levels, though this did not reach statistical

254 significance, and myelin stimulation robustly increased (~2-fold) TIMP2 release into the media
255 relative to unstimulated conditions (**Fig. 4d-e**).

256 Given that the brain accumulates abundant myelin debris with age[53], the increase in
257 TIMP2 in response to myelin stimulation motivated us to examine whether microglial TIMP2
258 modulates cellular response to myelin. We isolated adult microglia from tamoxifen-treated
259 *Cx3cr1*$^{CreERT2/+}$;*Timp2*$^{fl/fl}$ mice and *Timp2*$^{fl/fl}$ control mice and performed a myelin phagocytosis
260 assay in which myelin was conjugated with pHrodo red, a pH-sensitive dye that fluoresces in the
261 acidic endosomal/lysosomal compartment that was monitored over time using a live-cell imaging
262 system (**Fig. 4f**)[54]. 'Area under the curve' analysis revealed significantly lower uptake of myelin in
263 *Cx3cr1*$^{CreERT2/+}$;*Timp2*$^{fl/fl}$ microglia over a 12-hour period compared to the uptake observed in
264 control microglia (**Fig. 4g-h**). We next assessed the rate of myelin clearance in the two groups by
265 treating new cultures with myelin, followed by withdrawal of the treatment with fresh media to
266 measure the rate of myelin elimination (**Fig. 4i**). We observed a lower rate of myelin clearance in
267 *Cx3cr1*$^{CreERT2/+}$;*Timp2*$^{fl/fl}$ microglia relative to Timp2$^{fl/fl}$ control microglia (**Fig. 4j-k**). Together, these
268 results suggest that deletion of microglial TIMP2 impairs microglial phagocytosis of myelin.

269 We previously reported that neuron-derived TIMP2 released into the brain extracellular
270 space is critical for hippocampal plasticity[25]. We next asked whether this additional extrinsic
271 source from neurons can regulate microglial state by creating Syn$^{Cre/+}$;*Timp2*$^{fl/fl}$ and *Timp2*$^{fl/fl}$ mice
272 to target neuronal TIMP2 expression[25] and then performing confocal imaging to evaluate
273 microglial state using IBA1 and CD68 markers (**Fig. 4l**). Similar to our findings demonstrating that
274 targeting the microglial pool of TIMP2 affects microglial state (**Fig. 3h**), we find that neuronal
275 TIMP2 deletion significantly increases the number of IBA1^{+}CD68^{+} cells in the DG (**Fig. 4m-n**),
276 while the total number of microglia in this region was not affected by TIMP2 deletion
277 (**Supplementary Fig. 4a-b**). Together, our findings indicate that microglia are responsive to
278 modulation of extracellular levels of TIMP2, regardless of whether the source is from microglia or
279 neurons.

280

281 **Systemic TIMP2 treatment reduces age-associated microgliosis and modulates microglial**
282 **state**

283 Given our data suggesting that extrinsic sources of TIMP2 regulate microglial state *in vivo*, we
284 next asked whether extrinsic application of TIMP2 to aged primary microglia could directly affect
285 microglial state phenotypes observed in our KO models, independent of regulation from other cell
286 types. We first isolated microglia from 20-month-old WT mice and evaluated whether application
287 of TIMP2 altered the number of $IBA1^+CD68^+$ cells in the culture (**Fig. 5a**). Treating aged primary
288 microglia with TIMP2 reduced the number of $CD68^+$ cells relative to control conditions (**Fig. 5b-**
289 **c**), suggesting that TIMP2 can directly alter microglial state independent of its known effects on
290 other CNS cell types[23,25,55]. Based on our previous results demonstrating that TIMP2 enters the
291 brain from blood following systemic injection[16], we next asked whether systemic treatments with
292 TIMP2 in aged mice can regulate microglial state and function. Using the same dosing paradigm
293 we previously showed improves learning and memory in aged mice (**Fig. 5d**)[16], we injected aged
294 WT mice systemically with TIMP2 (50 μg/kg), and isolated brains to evaluate changes in microglia
295 after ~2.5 weeks of injections. Systemic TIMP2 treatment reversed the consistent increase in
296 microglial activation observed in our KO models, as reflected by the decreased number of
297 $IBA1^+CD68^+$ cells in the DG of TIMP2-treated aged mice compared to vehicle-treated aged mice
298 (**Fig. 5e-f**). We also detected a lower percentage of DG area occupied by CD68 staining, whereas
299 the treatment did not affect the total number of $IBA1^+$ cells (**Supplementary Fig. 5a-c**).

300 To characterize how aged microglia respond to TIMP2 treatment at the transcriptomic
301 level, we applied a single-nuclei RNA-sequencing (snRNA-seq) pipeline on hippocampi isolated
302 from a new cohort of vehicle- and TIMP2-treated 20-month-old mice, based on an established
303 method[56]. Following quality-control measures to remove ambient RNA, doublets, and poor-quality
304 nuclei, we obtained 60,436 nuclei for downstream analysis in which nuclei from each sample were
305 integrated and clustered using uniform manifold approximation and projection (UMAP)

306 (**Supplementary Fig. 5d**). Combining use of ScType for automated cell-type identification[57] and
307 thorough interrogation of top marker genes for each cluster, we identified CNS cell types expected
308 for the hippocampus (**Supplementary Fig. 5d-e**). We next subclustered cells identified as
309 microglia (2,831 nuclei; **Fig. 5g**) and noted significant shifts in the proportion of cells in subclusters
310 2, 5, and 6 in mice treated systemically with TIMP2 compared to vehicle-treated mice (**Fig. 5h**;
311 **Supplementary Fig. 5f**). To identify what processes characterize these TIMP2-shifted
312 subclusters, we performed IPA on the significant genes defining these subclusters and examined
313 expression levels of top marker genes. TIMP2 treatment increased the proportion of microglia in
314 subcluster 2, a cluster characterized by the highest expression of *Apoe,* a gene that regulates
315 phagocytosis and lipid uptake[28,58] (**Supplementary Fig. 5g**), as well as by iron handling ("uptake
316 and transport") and immune response processes ("cyclophilin signaling") (**Fig. 5i**). TIMP2
317 treatment shifted subcluster 1, albeit modestly (**Supplementary Fig. 5f**), which was characterized
318 by genes relating to phagosome formation and signaling in myeloid cells (**Supplementary Fig.
319 5h**). TIMP2 treatment significantly reduced the proportion of microglia in subcluster 5 (**Fig. 5h;
320 Supplementary Fig. 5f**), a cluster defined by "axon guidance signaling", "synaptogenesis
321 signaling", and "neurexins and neuroligins" (**Fig. 5j**). This subcluster, along with 2 other microglial
322 subclusters with neuron-associated genes, also had highly enriched expression of *Gria1*
323 (**Supplementary Fig. 5g**), a gene linked to microglial-neuron interactions[59,60]. Intriguingly, we
324 found that TIMP2 treatment resulted in a significant decrease in proportion of subcluster 6
325 microglia (**Fig. 5h; Supplementary Fig. 5g**), which were defined by pathways associated with
326 production of "nitric oxide and reactive oxygen species (ROS) in macrophages", "senescence",
327 "Fcγ receptor-mediated phagocytosis", "IL-3, IL-5, and GM-CSF signaling", and "HGF signaling"
328 (**Fig. 5k)**. Further analysis of subcluster 6 markers revealed "TNF" as a top upstream regulator
329 (**Fig. 5l**), activating proinflammatory[61-63] and senescence-associated[64] pathways through IL6,
330 IFNG, STAT1/STAT5A, IRF8, and TP53, as well as IL10 as a counter-regulatory response

331 protein[65], together suggesting that TIMP2 treatment of aged mice reduces the proportion of
332 microglia associated with a pro-inflammatory and senescent-like state.

333 Given these shifts in microglial subclusters following TIMP2 treatment, we next aimed to
334 compare overall microglial gene expression changes following TIMP2 treatment. We found that
335 TIMP2 treatment resulted in differentially expressed genes (DEGs; 196 upregulated, 68
336 downregulated) in the overall microglia cluster. *Cst3* and *Apoe* were the two most significantly
337 upregulated genes (**Fig. 5m**). *Apoe* is a well-characterized regulator of the DAM transcriptional
338 state[28] and is upregulated in microglia phagocytosing apoptotic neurons[58], while *Cst3* is localized
339 in the lysosome, where it regulates lysosomal homeostasis[66]. We also observed a change in
340 ferroptosis-associated *Fth1*[67] and genes linked to metabolism and inflammation, including
341 *Ndufa4*[68] and *Tmsb4x,* which negatively regulates NFκB signaling[69] (**Fig. 5m**). Pathway analysis
342 on the overall DEGs reflected changes in cytokine/chemokine and interferon signaling, as well as
343 altered uptake processes (ferroptosis), and potential changes in microglia-neuron interactions
344 (ERBB4 and ERBB2 signaling) (**Fig. 5n**). We performed pre-ranked Geneset enrichment analysis
345 (GSEA)[70] to determine if genes, ranked by signed fold-change*-$\log_{10}$*P*-value$_{adj}$, were enriched
346 within gene sets previously associated with different microglial states, including disease-
347 associated microglia (DAM)[28], lipid-associated macrophages (LAM)[71], which was identified as a
348 protective state in adipose tissue of mice on a high-fat diet[71], lipid-droplet-accumulating microglia
349 (LDAM)[12], activated response microglia (ARM)[72], interferon-related[73] and homeostatic microglia[72].
350 Interestingly, we found that TIMP2 treatment resulted in positive enrichment in LAM, DAM, and
351 ARM gene sets in microglia (**Fig. 5o; Supplementary Fig. 5i**), supporting a putative enrichment
352 in genes associated with protective response to damage.
353

354 **Systemic TIMP2 restores phagocytic capacity in aged microglia**

355 Phagocytic capacity of microglia is diminished in aging and in proinflammatory states[8,9,12,74], and
356 targeting this process may facilitate effective clearance of dead cells or debris[9,10,75]. Given the

357 TIMP2-induced changes observed in microglial phagocytosis-related pathways and in putative
358 microglial-synapse interactions in snRNA-seq experiments, we evaluated how systemic TIMP2
359 treatment affects the ability of microglia to phagocytose synaptic material in the DG. We
360 hypothesized that TIMP2 treatment elevates microglial phagocytosis in aged DG, especially given
361 our results showing that microglia-specific *Timp2* deletion reduced myelin phagocytosis (**Fig. 4g-**
362 **h**). To evaluate microglial phagocytosis in aged mice following TIMP2 or vehicle treatment (**Fig.**
363 **5d**), we performed confocal imaging of sections stained with antibodies for IBA1, CD68, and
364 synaptic marker VGLUT1, followed by Imaris-3D reconstruction to visualize lysosome-associated
365 synaptic puncta in individual microglia. We found that TIMP2 treatment increased the volume of
366 VGLUT1^{+} puncta within microglia lysosomes in the DG relative to vehicle treatment (**Fig. 5p-q**),
367 reflecting enhanced phagocytic function of a process typically diminished with aging[8,12].
368

369 **Discussion**

370 In the current study, we define a novel role of youth-associated protein TIMP2 in regulating
371 microglial state in the context of aging pathology and in normal brain homeostasis. Global,
372 microglial-specific, and neuronal-specific deletion of TIMP2 accelerated activation and associated
373 deleterious phenotypes of microglia in the hippocampus. TIMP2 also appeared to modulate the
374 phagocytic uptake and clearance of physiological substrates by microglia, including myelin, while
375 regulating the inflammatory state of these cells. Given that various sources of expression
376 contribute to the brain extracellular pool of TIMP2, we explored how systemic supplementation
377 with TIMP2 in aged mice affects microglia, which reversed many of the phenotypes associated
378 with TIMP2 removal, including microgliosis and impaired phagocytosis, while highlighting
379 transcriptomic shifts in microglia associated with deleterious microglial phenotypes. Together, our
380 results highlight that microglia are sensitive to extracellular levels of TIMP2, and that increasing
381 TIMP2 promotes a shift toward a more protective state that may counteract age-associated
382 pathology.

383 Early studies provided intriguing evidence that exposure to the systemic environment may
384 affect microglia[18,76] and that these cells can take up proteins originating in plasma[20,21], yet little is
385 known of the effects of such proteins on microglia. Specifically, recent work found that labeled
386 plasma proteins are found within microglia of healthy brains in a process that appears to involve
387 a specialized subset of microglia characterized by antigen presentation, as well as high metabolic
388 and phagocytic activity[21], though it remains unclear whether these processes diverge in the aged
389 brain. A further recent study identified PF4 as a platelet factor that modulates microglial state,
390 though it may not penetrate the brain appreciably and instead acts on peripheral T cells to
391 indirectly modulate the CNS[18,77], highlighting that microglia likely respond to blood-borne factors
392 through a variety of mechanisms. In the case of TIMP2, previous work found that labeled TIMP2
393 enters the brain after peripheral delivery in aged mice[16]. Our current data examining the impact
394 of neuronal, microglial, and systemic sources of TIMP2 on microglial phenotypes collectively
395 support the concept that extracellular pools of TIMP2 regulate microglial function.

396 A growing literature has highlighted roles for TIMP2 in regulating overall hippocampal
397 function by modulating synaptic plasticity mechanisms[16,25], raising the possibility that some of the
398 effects observed in microglia may reflect, in part, its action on neurons. While this remains a
399 possibility, we find that aged primary microglia treated with TIMP2 recapitulate phenotypes
400 observed in the intact brains of aged mice treated systemically with TIMP2, suggesting that
401 microglia are directly responsive to TIMP2. In terms of its molecular targets, a recent study using
402 a modified TIMP2 construct lacking MMP inhibitory activity was still sufficient to enhance
403 hippocampal plasticity phenotypes, arguing for non-canonical targets for TIMP2 activity[23] beyond
404 classical interactions with MMPs. Given the many distinct interactions for TIMP2 activity that have
405 been identified[24], future studies should focus on delineating molecular targets for specific CNS
406 functions.

407 To further examine how TIMP2 modulates microglial state, we applied a combination of *in*
408 *vivo* and *in vitro* approaches across multiple ages, which revealed a consistent phenotype of

409 heightened microglial activation in the setting of TIMP2 deficiency that is reversed with TIMP2
410 supplementation. To characterize the local extracellular environment, we implemented an *in vivo*
411 microdialysis method that permitted sensitive assessment of immune-related proteins, an
412 approach that revealed marked alterations in the extracellular milieu in factors related to
413 inflammation, lysosomal activity, and cellular stress responses, reflecting altered
414 neuroinflammatory environment. Our transcriptomic analysis of aged microglia from TIMP2-
415 treated mice largely corroborated these roles of TIMP2 as a driver of protective microglial states.
416 In microglia of aged mice treated with TIMP2, we find enrichments in sets of genes resembling
417 the LAM[71], DAM[28], and ARM[72] states associated with protective macrophage/microglia function.
418 DAM and ARM states are both associated with protective responses to aging and AD
419 pathology[28,72] while being characterized by elevated *Apoe* expression, a top upregulated gene in
420 TIMP2-treated microglia in our dataset. Several studies have demonstrated that these states, and
421 induction of genes associated with these states, are necessary for microglia to appropriately
422 respond to damage[28,58,72,78,79]. We also found significant enrichment in the LAM geneset in TIMP2-
423 treated microglia, which has been argued to be a protective myeloid state in adipose tissue of
424 mice on a high-fat diet[71]. These macrophages are involved in phagocytosis, lipid catabolism, and
425 energy metabolism[71], largely fitting with our observed upregulation of genes related to
426 phagocytosis, metabolism, and modulation of inflammatory response in microglia from TIMP2-
427 treated mice. The enrichment in genes associated with LAM, DAM, and ARM states with TIMP2
428 treatment may reflect a shared change in microglial response to lipid-rich damage, including the
429 myelin debris encountered by aged microglia, possibly a protective response to aging that is
430 bolstered with TIMP2 treatment. Corroborating the protective effects, we see a corresponding
431 loss of microglial subpopulations characterized by deleterious pathways in microglia from TIMP2-
432 treated mice, including senescence, production of nitric oxide and ROS, and pro-inflammatory
433 programs driven by TNF. A previous *in vitro* study using the BV2 cell line suggested that TIMP2

434 may have anti-inflammatory roles, including production of IL10 and reduction of pro-inflammatory
435 cytokines following LPS stimulation[80], supporting our *in vivo* observations.

436 A consistent phenotype we observed across experiments modulating TIMP2 levels is the
437 shift in microglial activation and associated lysosomal and phagocytic capacity. Using lysosomal-
438 associated marker CD68, we show that removing TIMP2 increases activation state, while
439 reducing uptake and removal of myelin, together supporting that TIMP2 regulates how
440 physiological material is removed from the extracellular space. Interestingly, by sampling the brain
441 extracellular space of mice lacking TIMP2, we detected elevations in the lysosomal serine
442 protease TPP1, perhaps reflecting response to aberrant debris removal by microglia, a
443 phenomenon observed under conditions of lysosomal stress[81,82]. Conversely, TIMP2 treatment of
444 aged mice reduces microglial activation and increases phagocytic capacity—a function typically
445 diminished with age and under proinflammatory conditions[8,9,74]. These data dovetail with our
446 transcriptomic data from treated aged mice that reveal upregulation of genes involved in
447 phagocytic processes and metabolism and a shift away from proinflammatory microglial states,
448 perhaps reflecting a more efficient endolysosomal capacity. In addition to the benefit of clearing
449 debris to protect the local brain environment, the process of phagocytosis itself can also inhibit
450 proinflammatory responses[83], though future work will need to identify the directionality of these
451 changes following treatment with TIMP2 and related factors. Together, this work suggests that
452 TIMP2 modulates the ability of microglia to remove extracellular material, enabling them to more
453 effectively engage in phagocytosis while reducing the inflammatory environment in the setting of
454 age-related pathology.

455

456 Our findings demonstrate that TIMP2 modulates microglial state, enhancing phagocytic function
457 and dampening inflammatory activation in the aged brain. By promoting a more protective set of
458 microglial phenotypes, TIMP2 may help counteract accumulation of debris and chronic
459 inflammation that characterize the aged CNS environment. Given that genetic risk for AD is

460 enriched in genes involved in microglial phagocytosis and endolysosomal function[84], future
461 studies should explore how TIMP2 influences these pathways in contexts of aging and age-
462 related neurodegenerative conditions. Together, our work positions TIMP2 as a promising
463 candidate for mitigating microglial dysfunction and preserving brain health across the lifespan.

464 **Materials and Methods**

465

466 **Animals**

467 Animal procedures, care, and handling were performed in accordance with the NIH Guide for
468 Care and Use of Laboratory Animals and the Icahn School of Medicine at Mount Sinai Institutional
469 Animal Care and Use Committee. All mice were maintained on C57Bl/6 background. TIMP2 -/-
470 (KO) mice were purchased from Jackson Laboratory, and 5xFAD mice were purchased from
471 MMRRC and subsequently maintained in-house alongside WT littermates. *Timp2*$^{fl/fl}$ mice were
472 generated as previously described[25] and crossbred with *Cx3cr1*$^{CreERT2/+}$*Lit51t* mice or Syn$^{Cre/+}$ lines
473 (Jackson) to permit microglial and neuronal deletion[25] of TIMP2, respectively. To induce
474 conditional deletion of microglial *Timp2*, 2-month-old mice were administered 100 mg/kg
475 tamoxifen (Sigma Aldrich Fine Chemicals Biosciences, T5648) in corn oil (Sigma, C8267) 5 times
476 by oral gavage, with at least 48-h separation between gavages[78]. Cre-negative *Timp2*$^{fl/fl}$
477 littermates were also given tamoxifen as controls. Aged WT C57BL/6 mice were obtained from
478 the National Institute on Aging aged rodent colony. Male and female mice were used unless
479 otherwise indicated.

480

481 **Neonatal microglia isolation**

482 Using an established protocol[85], we dissected forebrain from pups (P5-P8) and manually
483 homogenized the tissue using a dounce homogenizer (VWR, KT885300-0002), prior to debris
484 removal using a 20% Percoll gradient (GE Healthcare, 17-0891-02). Microglia were positively
485 selected using CD11b microbeads (Miltenyi Biotec, 130-049-601), LS columns (Miltenyi Biotec,
486 130-042-401), and a QuadroMACS Separator according to manufacturer instructions. For
487 western blot analysis, cell pellets were collected and frozen at -80C until use. For ICC and bulk
488 RNAseq experiments, cells were manually counted with a hemacytometer and Trypan blue
489 staining to assess cell viability. Cells were plated at a density of 200,000 microglia/well in 96-well

490 poly-d-lysine-coated plates (Corning, 354461) in Dulbecco's modified Eagle's medium (DMEM)
491 supplemented with 10% FBS (Sigma, F4135, Sigma) and 1% penicillin–streptomycin (Gibco,
492 15140). Microglia recovered for a minimum of 2 days in tissue culture incubator before
493 experiments.
494
495 **Adult microglia isolation**
496 Following an established protocol[52], mice were perfused with ice-cold PBS, cerebellum and
497 olfactory bulbs were removed, and remaining brain tissue was enzymatically dissociated using
498 the Neural Tissue Dissociation Kit (P) (Miltenyi Biotech, 130-092-628) according to manufacturer
499 instructions. During incubation in enzymatic buffer, large, medium, and small fire polished Pasteur
500 pipettes were used to mechanically dissociate tissue. Following filtration and centrifugation,
501 samples were incubated with CD11b microbeads (Miltenyi Biotec 130-049-601) and subsequently
502 separated using LS columns (Miltenyi Biotec 130-042-401) and QuadroMACS Separator using
503 manufacturer's instructions. Cells were plated on imaging plates (Cellvis, P96-1.5H-N) or poly-L-
504 Lysine-coated glass coverslips (Electron Microscopy Sciences, 72292-04) in DMEM
505 supplemented with 10% FBS and 1% penicillin–streptomycin. Microglia were allowed to recover
506 for 7 days in a tissue culture incubator before experiments. Wells were excluded from analysis if
507 cultures did not meet viability or quality control criteria (e.g. excessive debris).
508
509 ***In vitro* phagocytosis assay**
510 Following a 7-day recovery period post-isolation, conditioned media from primary microglial
511 cultures was removed and replaced with serum-free media before measurements in the IncuCyte
512 S3 live-cell analysis system (Sartorius) that contained a tissue culture incubator at 37C/5% CO2
513 for baseline imaging. Cells were treated with pHrodo-labeled myelin[54] (10 μg/mL), generously
514 provided by the laboratory of Dr. Alison Goate, and imaged hourly at 20x using phase contrast
515 and red fluorescent signal. For myelin clearance experiments, following a 3-hour incubation with

516 pHrodo-labeled myelin, cells were washed with PBS and fresh serum-free media was added that
517 did not contain myelin. Total integrated density was calculated by multiplying the average red
518 object mean intensity (RCU, red calibrated units) by the average phase object area (cell, μm^2)
519 and plotted over time[86]. For both uptake and clearance experiments, two independent
520 experiments were conducted with 3 technical replicates per animal that were averaged.
521
522 ***In vitro* microglial stimulation**
523 To assess TIMP2 secretion with various substrates, cultures of adult WT microglia were
524 stimulated with various substrates in serum-free media at the following concentrations: Zymosan
525 10 μg/mL, myelin 10 μg/mL, LPS 100 ng/mL, or PBS control. 12 hours following stimulation,
526 conditioned media was collected and concentrated for immunoblotting. For experiments
527 examining activation of primary microglia from aged mice following TIMP2 treatment, cell media
528 was replaced with serum-free media 2 hours prior to incubation with TIMP2 (2 μg/mL, R&D
529 Systems, 6304-TM-010) or vehicle (PBS) for 28 hours, after which cells were fixed and stained to
530 evaluate markers.
531
532 **Bulk RNA-sequencing of neonatal microglia**
533 Forebrains from neonatal mice were pooled by genotype, and then microglia were isolated and
534 plated in 12-well poly-d-lysine-coated plates (Corning, 354470) at a density of 600,000 cells per
535 well, 2 wells per genotype. After 72 hours, trypsin was used to remove cells prior to centrifugation
536 for 5 minutes at 1230 x g, followed by resuspension in PBS, and re-centrifugation. Pellets were
537 stored at -80C before further processing and sequencing by Genewiz (Azenta) with each sample
538 representing independent isolations from pooled pups. RNA was extracted and quality was
539 measured using TapeStation Analysis Software 3.2 (Agilent), and concentration was determined
540 using Qubit assay, with all samples exhibiting RNA Integrity Number (RIN) = 10. Sequencing

541 libraries were prepared with poly(A) selection and sequenced using Illumina Hiseq (2x150bp
542 paired-end) according to manufacturer protocols. Reads were mapped to the Mus musculus
543 GRCm38 genome. Differential expression was performed using DESeq2, and differentially
544 expressed genes (P<0.05) were used to perform Ingenuity Pathway Analysis (IPA, Qiagen), as
545 well as gene ontology over-representation analysis with the MSigDB[31] database on significantly
546 upregulated and downregulated genes separately.
547
548 **Immunoblotting**
549 To perform western blot analysis of TIMP2 in primary microglia, cell pellets from pooled samples
550 were lysed in RIPA buffer (Thermo Fisher) containing protease Inhibitor cocktail (Roche) for 30
551 min on ice, collecting lysates following a 30-min centrifugation at 15,000 x g. 80 μg of protein per
552 sample was loaded on Bolt 4-12% Bis-Tris Plus Gels (Invitrogen). TIMP2 from conditioned media
553 was spun at 1,000 x g for 10 min to remove debris. Protease inhibitor cocktail was added to
554 supernatant prior to concentration of media by centrifugation at 4,000 x g for 40 min using Amicon
555 Ultra-15 centrifugal filter unit (Amicon, UFC901024) before loading on 4-12% NuPAGE Bis-Tris
556 denaturing gels (Invitrogen). Gels were transferred, the blots probed with anti-TIMP2 (1:5000;
557 D18B7, Cell Signaling) or anti-actin (1:10000; A5060; Sigma), and then developed as previously
558 described[25], with multiple blots per experiment developed in parallel where necessary. Band
559 intensities were quantified using ImageJ software as described[41].
560
561 **Immunocytochemistry**
562 Following fixation with 4% paraformaldehyde for 20 min at room temperature, primary microglia
563 were washed three times with PBS, incubated with blocking solution (10% donkey serum and
564 0.1% triton-X in PBS) for 1 hour, and then incubated overnight at 4C with primary antibodies in
565 blocking solution at the following concentrations: IBA1, 1:500, (019-19741, Wako); CD68, 1:200,
566 (MCA1957, BioRad), TIMP2, 1:100 (AF971, R&D systems, [2-day incubation]), p16INK4a, 1:500,

567 (MA5-17142, Invitrogen). Cells were then washed and incubated in their corresponding secondary
568 antibody for 1 hour. Staining was visualized and imaged using the Keyence BZ-X700 microscope
569 or Zeiss LSM780 upright confocal microscope using a 40x objective. 2-3 wells per mouse were
570 plated and 3-4 images per well were averaged for 3 technical replicates per mouse. The value for
571 each mouse represents the mean of these replicates.
572
573 **Immunohistochemistry and imaging**
574 Following anesthetization with a ketamine (90 mg/kg) and xylazine (10 mg/kg) cocktail, mice were
575 perfused transcardially with ice-cold 0.9% saline. Brains were dissected and postfixed in 4%
576 paraformaldehyde for 48 hours and then preserved with 30% sucrose in PBS. 40-μm sections
577 were prepared from hemibrains and sectioned using a freezing-sliding microtome and stored at -
578 20C in cryoprotectant media prior to immunohistochemistry according to our previous protocol[16].
579 Briefly, free-floating sections were blocked in appropriate serum (10%) before incubation in
580 primary antibody at 4C overnight. Primary antibodies were used at the following concentrations:
581 IBA1, 1:500, (Wako, 019-19741); CD68, 1:200, (MCA1957, BioRad); VGLUT1, 1:2000, (135318,
582 Synaptic Systems); CD68, 1:500, (137001, BioLegend, paired with IBA1 and VGLUT1 co-
583 staining). Sections were then incubated in the corresponding fluorescently-conjugated secondary
584 antibodies for 1 hour (1:200 in TBST), followed by DAPI, where indicated, for 15 min. Stained
585 sections were mounted and coverslipped with ProLong Gold (Invitrogen).
586 To image staining in the dentate gyrus, 2x2 tile-scanning images were acquired through
587 the entire z-plane of sections (1-μm intervals across ~40μm) at 40x/1.4 oil DIC objective using a
588 Zeiss LSM780 upright confocal microscope. For all imaging experiments, 3-4 sections per animal
589 were imaged according to stereological principles, as previously described[16]. FIJI was used to
590 perform thresholded “percentage area” or count analysis of cells expressing CD68 and/or IBA1
591 across mouse experiments in a blinded fashion. Count data was normalized to the area of the
592 analyzed ROI.

593 *Imaris-based imaging and analysis*

594 Following IHC for VGLUT1, IBA1, and CD68, images containing dentate gyrus were acquired
595 using a 63X oil-immersion objective lens on a Zeiss LSM780 with 0.33-μm z-step size across ~20-
596 μm z-stack (1024x1024 pixels). 3D reconstruction of microglia was performed using Imaris (Imaris
597 10.2, Oxford Instruments). Microglial surfaces were created using machine learning-based
598 training on the IBA1 channel, which were then used to mask the CD68 channel. A surface was
599 then created for the microglial-masked CD68 and used to mask VGLUT1 signal. A surface for
600 VGLUT1 signal within a microglial lysosome was created, together creating $VGLUT1^+$ surfaces
601 within a microglial lysosome. The total volume of VGLUT1 within lysosomes was normalized to
602 the volume of the microglial surface analyzed. Three sections per mouse were imaged, and
603 results for microglia were averaged to represent a value for each mouse. A total of 44-47 microglia
604 were analyzed per group.

605 *Microglia morphology analysis*

606 We employed an established protocol defining microglia morphologies based on their circularity
607 ($(4\pi \text{ Area}) / \text{Perimeter}^2$) assessed by FIJI, where values approaching a value of 1 approximate a
608 circular morphology[33-36]. "Ramified" morphology was categorized according to circularity between
609 0 and 0.400, "activated/reactive" microglia are defined by circularity of 0.500-0.699, and
610 "ameboid" morphology are defined by circularity of 0.700-1.000. Images were imported to FIJI,
611 converted to 8-bit, background-corrected (rolling ball radius of 50 pixels and despeckled) equally
612 across images/groups, and then classified into the three morphology types according to
613 circularity. The number of microglia corresponding to each morphology class was normalized to
614 stereologically-defined dentate gyrus areas.

615

616 **Recombinant protein injections**

617 For experiments in which mice were treated systemically with TIMP2, aged mice were given
618 intraperitoneal (i.p.) injections every other day with either vehicle (PBS) or recombinant mouse
619 TIMP2 (R&D Systems, 6304-TM-010) for a total of 8 injections, using our established protocol, a
620 method used previously to provide revitalization of hippocampal plasticity and cognitive function[16].
621

622 **Nuclei Isolation and snRNA-seq**

623 Full hippocampi were isolated, flash-frozen, and stored at -80C until processing. Hippocampi were
624 thawed on ice, and nuclei were isolated using established protocols[56]. Briefly, each hippocampi
625 was mechanically dissociated using a dounce homogenizer (VWR) with 2 ml of EZ lysis buffer
626 (Millipore Sigma). Samples were centrifuged, resuspended in fresh lysis buffer, and centrifuged
627 again. Cell pellets were gently washed with 4 ml ice-cold PBS, and supernatant were removed
628 prior to resuspending pellets in 100 µl of ice-cold PBS with 0.04% BSA (NEB) and 1 U/µL RNAse
629 inhibitor (Millipore Sigma). Each sample was filtered through 40-µm FlowMi cell strainers
630 (Millipore), and nuclei were counted (aided by trypan blue) to assess nuclei viability using an
631 EVOS M7000. Two biological samples from the same treatment condition were pooled to load
632 20,000 nuclei total (10,000 nuclei each) for a total N=2 samples per treatment condition. Libraries
633 were prepared and sequenced by the Single-cell & Spatial Technologies Team, Center for
634 Advanced Genomics Technology Genomics Core (ISMMS) using the 10x Genomics Chromium
635 platform for library preparation (V2 3' GEX protocol) according to manufacturer's instructions.
636 Briefly, cDNA was extracted from Gel-Bead in Emulsions (GEMs) obtained from the sample chip
637 in the Chromium controller, and library quality control was performed with MiSeq Nano. Libraries
638 were run on Illumina NovaSeq 6000 S4 Flowcell (2x100 nt paired-end read length) configuration,
639 targeting 50,000 reads per cell.

640 Raw read data was analyzed by 10x Cell Ranger (v7.1.0) to align to reference genome
641 (Mus musculus, version mm10 2020-A). Downstream processing was performed in the R
642 programming environment (v4.2.0 or v4.4.2). Ambient RNA was removed from samples using

643 SoupX[87] and manual application of a stringent contamination fraction on a per sample basis. After
644 initial filtering, doublets were identified and removed using DoubletFinder[88]. Further filtering
645 involved removing genes expressed in fewer than 3 cells, cells with a UMI count under 500, and
646 cells with only 500 genes per cell to ensure we analyzed high-quality cells. The Seurat object was
647 then log-normalized, and variable features were identified using the FindVariableFeatures
648 function. ScaleData was then used to regress cells with more than 2% mitochondrial, ribosomal
649 large subunit (RPL) and ribosomal small subunit (RPS) gene expression content. Using STACAS,
650 a semi-supervised data integration method, we integrated all samples[89], which was used for cell
651 clustering. Using Seurat (v5.2.1), integrated samples were scaled, and clusters were identified
652 using FindNeighbors (using top 50 principal components) and FindClusters (Resolution=0.25). To
653 identify markers of each cluster, the RNA assay was processed using NormalizeData,
654 FindVariableFeatures, ScaleData (regressing out > 2% mitochondria, RPS, and RPL), and
655 FindMarkers. We determined cluster identity by assessing the top 30 markers on DropViz, further
656 confirming identities with ScType[57] and by examining literature-based expression of marker genes
657 for each cell type. Clusters identified to be microglia were subclustered (using the top 15 principal
658 components and a resolution of 0.5). Clusters suspected as containing doublets, i.e., marked by
659 high nCount_RNA and nFeature_RNA, as well as a lack of microglial genes as cluster markers,
660 were removed, and the remaining cells were re-clustered using the top 15 principal components
661 and a resolution of 1. Pathways representing each subcluster were evaluated using the
662 significantly upregulated marker genes in each subcluster ($P_{adj} < 0.05$; via FindAllMarkers) and
663 by running these markers in Ingenuity Pathway Analysis (IPA, Qiagen) and gene ontology over-
664 representation analysis using MSigDB[31]. To compare shifts in the proportion of subclustered cells
665 between treatment conditions, we employed scProportionTest[90].

666 Differential gene expression analysis for the microglia cluster was conducted using
667 DESeq2, and IPA was run on significant genes ($P_{adj} < 0.05$). After removing genes not mapping
668 to Entrez identifiers, we performed GSEA using a ranked list of all genes tested in the differential

669 expression analysis to assess enrichment in published gene sets representing characterized
670 microglial states[70]. GSEA was performed in R using the clusterProfiler[91] package (v4.14.6),
671 implementing the Fast GSEA (fgsea) algorithm with default parameters[92]. The Benjamini-
672 Hochberg correction method was applied to adjust for multiple comparisons for differential
673 expression and pathway analyses.
674
675 **1-MDa *in vivo* microdialysis**
676 Stereotaxic surgery and 1-MDa *in vivo* microdialysis was performed as previously described[25].
677 Mice were anesthetized with 2% isoflurane, and the head was shaved and fixed in a stereotaxic
678 apparatus (Stoelting Co.). Skull position was leveled, and a hole was drilled at bregma -3.1 mm,
679 2.5 mm lateral to target the left caudal hippocampus. Another hole was made diagonal to the first
680 to position an anchoring bone screw. After meninges were removed, an AtomosLM Guide
681 Cannula (PEG-12, Eicom) was inserted at a 12° angle, 1.2 mm below the brain surface at the
682 target location. The cannula was secured, and skin was closed using dental cement and surgical
683 adhesive glue. An AtmosLM Dummy Cannula (PED-12, Eicom) was inserted into the guide
684 cannula and secured with a plastic cap nut as the animal recovered in a clean cage on a heating
685 pad. Approximately 12 hours following surgery, 1-MDa *in vivo* microdialysis probes (AtmosLM;
686 Emicon) were inserted into caudal hippocampus. To calibrate the system prior to probe insertion,
687 inlet tubing (FEP tubing 0.65 mm OD x 0.12 mm ID, BASi) was connected to a syringe pump
688 (KdScientific) that perfused artificial cerebrospinal fluid (aCSF) containing, in mM: 1.3 $CaCl_2$, 1.2
689 $MgSO_4$, 3 KCl, 0.4 KH_2PO_4, 25 $NaHCO_3$, 122 NaCl, pH 7.35, at a rate of 1.2 µl/min. The outlet
690 tubing was connected to a peristaltic pump (MAB 20, SciPro), which was carefully calibrated to
691 obtain a pull rate between 0.9-1.1 µl/min. Probe integrity was tested, and once passing initial
692 quality control, it was connected to the inlet and outlet ports. The push-pull system was connected
693 to the probe and allowed to equilibrate prior to implanting in mouse brain. The probe was secured
694 with a cap-nut, and mice were placed in a Raturn (Stand-Alone Raturn System, BASi) and

695 tethered by a loose collar to enable free movement while preventing tangling of microdialysis
696 tubing. Dialysate from brain ISF was collected hourly at ~1.0 µl/min into a refrigerated fraction
697 collector (MAB 85 Fraction Collector, SciPro) and frozen at −80°C after collection for pooling and
698 subsequent measurement. In microdialysis experiments involving LPS administration, mice were
699 given a single i.p. injection of LPS (5 mg/kg in PBS), and samples were collected for an additional
700 10hrs. For all experiments, mice were given *ad libitum* access to food and water and were kept
701 under constant light conditions to minimize the impact of circadian protein flux, as previously
702 described[93].
703
704 **Protein analysis from ISF dialysates**
705 Hippocampal ISF dialysate samples were thawed on ice and pooled for measurements. For WT
706 and TIMP2 KO comparisons, samples representing the stable 24-hour steady-state period were
707 pooled within each mouse for subsequent measurements. For LPS experiments, the period
708 representing a stable baseline over a 12-hour period were pooled within each mouse to serve as
709 the pre-LPS sample per mouse. Samples corresponding to hours six to ten following LPS
710 treatment were pooled within each mouse to serve as the post-LPS treatment samples per
711 mouse. For all experiments, 230 µl of pooled sample was concentrated approximately 6-fold by
712 centrifugation at 14,000 x g for 75 min at 4C with a concentrator unit (Amicon Ultra-0.5 Centrifugal
713 Filter Units (MilliporeSigma). 25 µl of concentrated sample was loaded on a 96-well plate using
714 the Olink Target Mouse Exploratory Panel, encompassing cytokines and chemokines (Olink,
715 Uppsala Sweden) in coordination with the Human Immune Monitoring Center (ISMMS). Data was
716 represented as Normalized Protein EXpression (NPX) unit on a log2 scale.
717
718 **Statistical analysis**

719 Statistics were performed using GraphPad Prism version 10 (GraphPad Software) or R
720 programming environment (version 4.4.2 or version 4.2.0) using tests described in figure legends.
721 All relevant statistical tests were two-sided.
722

723 **Acknowledgements**

724 We would like to thank Anna Podlesny-Drabiniok, Michael Sewell, Raphael Kubler, and Mikaela
725 Rosen for advice related to snRNA-sequencing analysis, Eva Czirr for adult microglia isolation
726 and culturing advice, Hanxiao Liu and Jeffrey Zhu for technical support, and Swastik P. G. for
727 morphology advice. We thank Sanjana Shroff and Kristin Beaumont for assistance regarding
728 snRNAseq (Single Cell Genomics Core, ISMMS), the Human Immune Monitoring Center
729 (ISMMS) for Olink measurements, and Deanna Benson and Nikos Tzavaras of the Microscopy
730 CoRE and Advanced Bioimaging Center (ISMMS) for advice related to brain phagocytosis
731 imaging and analysis using Imaris software. Components of some figure panels used BioRender
732 content (https://BioRender.com/7o21lrw). We acknowledge computational and data resources
733 provided by Scientific Computing and Data (ISMMS), supported by the National Center for
734 Advancing Translational Sciences, UL1TR004419, and NIH grants S10OD026880 and
735 S10OD030463. This work was supported by the National Institute on Aging (R01AG061382
736 (JMC), RF1AG072300 (JMC),1F31AG079604-01A1 (BMH), T32AG049688 (BMH, SMP), and
737 R01AG061382-02S1 (JMC, SMP)).
738

739 **Author contributions**

740 BMH and JMC conceived and designed experiments, performed data analysis and interpretation,
741 and wrote the manuscript. BMH performed experiments. JMC supervised the research. ACF
742 generated tissue related to neuron-specific TIMP2 deletion, and some tissue for WT and TIMP2
743 KO mice, with percentage area and activation analysis for select cohorts, aided by AP. SMP
744 dissected hippocampi for sequencing experiments and provided additional expertise to guide

745 sequencing analysis. SFP performed morphology analysis and assisted with tissue isolation for
746 adult microglial cultures. All authors provided input and approved the paper.
747
748 **Competing interests**
749 J.M.C. is listed as a co-inventor on patents for treatment of aging-associated conditions, including
750 use of young plasma administration (US10688130B2) or youth-associated protein TIMP2
751 (US10617744B2), the latter of which was licensed to Alkahest, Inc.
752
753 **References**
754

755 1 Lau, V., Ramer, L. & Tremblay, M.-È. An aging, pathology burden, and glial senescence
756 build-up hypothesis for late onset Alzheimer's disease. *Nature Communications* **14**, 1670
757 (2023).
758 2 Romero-Molina, C., Garretti, F., Andrews, S. J., Marcora, E. & Goate, A. M. Microglial
759 efferocytosis: Diving into the Alzheimer's disease gene pool. *Neuron* **110**, 3513-3533
760 (2022).
761 3 Streit, W. J., Braak, H., Xue, Q.-S. & Bechmann, I. Dystrophic (senescent) rather than
762 activated microglial cells are associated with tau pathology and likely precede
763 neurodegeneration in Alzheimer's disease. *Acta Neuropathologica* **118**, 475-485 (2009).
764 4 Streit, W. J., Sammons, N. W., Kuhns, A. J. & Sparks, D. L. Dystrophic microglia in the
765 aging human brain. *Glia* **45**, 208-212 (2004).
766 5 Hu, Y. *et al.* Replicative senescence dictates the emergence of disease-associated
767 microglia and contributes to Aβ pathology. *Cell Reports* **35**, 109228 (2021).
768 6 Flury, A. *et al.* A neurodegenerative cellular stress response linked to dark microglia and
769 toxic lipid secretion. *Neuron* (2024).

770 7 Brelstaff, J. H. *et al.* Microglia become hypofunctional and release metalloproteases and
771 tau seeds when phagocytosing live neurons with P301S tau aggregates. *Sci Adv* **7**,
772 eabg4980 (2021).
773 8 Thomas, A. L., Lehn, M. A., Janssen, E. M., Hildeman, D. A. & Chougnet, C. A. Naturally-
774 aged microglia exhibit phagocytic dysfunction accompanied by gene expression changes
775 reflective of underlying neurologic disease. *Scientific Reports* **12**, 19471 (2022).
776 9 Heneka, M. T. *et al.* NLRP3 is activated in Alzheimer's disease and contributes to
777 pathology in APP/PS1 mice. *Nature* **493**, 674-678 (2013).
778 10 Zhou, Y. *et al.* Demyelination-derived lysophosphatidylserine promotes microglial
779 dysfunction and neuropathology in a mouse model of Alzheimer's disease. *Cellular &*
780 *Molecular Immunology* **22**, 134-149 (2025).
781 11 Hickman, S. E., Allison, E. K. & El Khoury, J. Microglial Dysfunction and Defective β-
782 Amyloid Clearance Pathways in Aging Alzheimer's Disease Mice. *The Journal of*
783 *Neuroscience* **28**, 8354-8360 (2008).
784 12 Marschallinger, J. *et al.* Lipid-droplet-accumulating microglia represent a dysfunctional
785 and proinflammatory state in the aging brain. *Nat Neurosci* **23**, 194-208 (2020).
786 13 Qin, L., Liu, Y., Hong, J. S. & Crews, F. T. NADPH oxidase and aging drive microglial
787 activation, oxidative stress, and dopaminergic neurodegeneration following systemic LPS
788 administration. *Glia* **61**, 855-868 (2013).
789 14 Castellano, Joseph M. Blood-Based Therapies to Combat Aging. *Gerontology* **65**, 84-89
790 (2019).
791 15 Bieri, G., Schroer, A. B. & Villeda, S. A. Blood-to-brain communication in aging and
792 rejuvenation. *Nature Neuroscience* **26**, 379-393 (2023).
793 16 Castellano, J. M. *et al.* Human umbilical cord plasma proteins revitalize hippocampal
794 function in aged mice. *Nature* **544**, 488-492 (2017).

795 17 Villeda, S. A. *et al.* Young blood reverses age-related impairments in cognitive function
796 and synaptic plasticity in mice. *Nature Medicine* **20**, 659-663 (2014).
797 18 Schroer, A. B. *et al.* Platelet factors attenuate inflammation and rescue cognition in ageing.
798 *Nature* **620**, 1071-1079 (2023).
799 19 Katsimpardi, L. *et al.* Vascular and Neurogenic Rejuvenation of the Aging Mouse Brain by
800 Young Systemic Factors. *Science* **344**, 630-634 (2014).
801 20 Yang, A. C. *et al.* Physiological blood–brain transport is impaired with age by a shift in
802 transcytosis. *Nature* **583**, 425-430 (2020).
803 21 Lu, N. *et al. Circulatory proteins shape microglia state and boost phagocytosis* (Cold
804 Spring Harbor Laboratory, 2024).
805 22 Anastasi, F. *et al.* Polygenic proxies of age-related plasma protein levels reveal TIMP2
806 role in cognitive performance. *Res Sq* (2024).
807 23 Britton, R. *et al.* Noncanonical Activity of Tissue Inhibitor of Metalloproteinases 2 (TIMP2)
808 Improves Cognition and Synapse Density in Aging. *eneuro* **10**, ENEURO.0031-0023.
809 (2023).
810 24 Peeney, D. *et al.* Mapping Extracellular Protein–Protein Interactions Using Extracellular
811 Proximity Labeling (ePL). *Journal of Proteome Research* **23**, 4715-4728 (2024).
812 25 Ferreira, A. C. *et al.* Neuronal TIMP2 regulates hippocampus-dependent plasticity and
813 extracellular matrix complexity. *Molecular Psychiatry* **28**, 3943-3954 (2023).
814 26 Nguyen, P. T. *et al.* Microglial Remodeling of the Extracellular Matrix Promotes Synapse
815 Plasticity. *Cell* **182**, 388-403.e315 (2020).
816 27 Cornell, J., Salinas, S., Huang, H.-Y. & Zhou, M. Microglia regulation of synaptic plasticity
817 and learning and memory. *Neural Regeneration Research* **17** (2022).
818 28 Keren-Shaul, H. *et al.* A Unique Microglia Type Associated with Restricting Development
819 of Alzheimer's Disease. *Cell* **169**, 1276-1290.e1217 (2017).

820 29 Almanzar, N. *et al.* A single-cell transcriptomic atlas characterizes ageing tissues in the
821 mouse. *Nature* **583**, 590-595 (2020).
822 30 Yao, Z. *et al.* A high-resolution transcriptomic and spatial atlas of cell types in the whole
823 mouse brain. *Nature* **624**, 317-332 (2023).
824 31 Liberzon, A. *et al.* The Molecular Signatures Database (MSigDB) hallmark gene set
825 collection. *Cell Syst* **1**, 417-425 (2015).
826 32 Shea, J. M. & Villeda, S. A. Microglia aging in the hippocampus advances through
827 intermediate states that drive activation and cognitive decline. *eLife* **13**, RP97671 (2025).
828 33 Oliveros, G. *et al.* Repurposing ibudilast to mitigate Alzheimer's disease by targeting
829 inflammation. *Brain* **146**, 898-911 (2022).
830 34 Avila, J. A. *et al.* PACAP27 mitigates an age-dependent hippocampal vulnerability to
831 PGJ2-induced spatial learning deficits and neuroinflammation in mice. *Brain and behavior*
832 **10**, e01465 (2020).
833 35 Chaudry, O. *et al.* Females exhibit higher GluA2 levels and outperform males in active
834 place avoidance despite increased amyloid plaques in TgF344-Alzheimer's rats. *Scientific*
835 *Reports* **12**, 19129 (2022).
836 36 Corwin, C. *et al.* Prostaglandin D2/J2 signaling pathway in a rat model of
837 neuroinflammation displaying progressive parkinsonian-like pathology: potential novel
838 therapeutic targets. *Journal of Neuroinflammation* **15** (2018).
839 37 Ulrich, J. D. *et al.* In vivo measurement of apolipoprotein E from the brain interstitial fluid
840 using microdialysis. *Molecular Neurodegeneration* **8**, 13 (2013).
841 38 Pait, M. C. *et al.* Novel method for collecting hippocampal interstitial fluid extracellular
842 vesicles (EV(ISF)) reveals sex-dependent changes in microglial EV proteome in response
843 to Abeta pathology. *J Extracell Vesicles* **13**, e12398 (2024).

844 39 Lund, S. *et al.* The dynamics of the LPS triggered inflammatory response of murine
845 microglia under different culture and in vivo conditions. *Journal of Neuroimmunology* **180**,
846 71-87 (2006).
847 40 Cirrito, J. R. *et al.* In Vivo Assessment of Brain Interstitial Fluid with Microdialysis Reveals
848 Plaque-Associated Changes in Amyloid-β Metabolism and Half-Life. *The Journal of*
849 *Neuroscience* **23**, 8844-8853 (2003).
850 41 Castellano, J. M. *et al.* Human apoE isoforms differentially regulate brain amyloid-β
851 peptide clearance. *Sci Transl Med* **3**, 89ra57 (2011).
852 42 Lively, S. & Schlichter, L. C. Microglia responses to pro-inflammatory stimuli (LPS, IFNγ+
853 TNFα) and reprogramming by resolving cytokines (IL-4, IL-10). *Frontiers in cellular*
854 *neuroscience* **12**, 215 (2018).
855 43 Barbera, M. C. *et al.* Increased ectodysplasin-A2-receptor EDA2R is a ubiquitous hallmark
856 of aging and mediates parainflammatory responses. *Nature Communications* **16** (2025).
857 44 Tsuboi, Y. *et al.* Increased hepatocyte growth factor level in cerebrospinal fluid in
858 Alzheimer's disease. *Acta Neurol Scand* **107**, 81-86 (2003).
859 45 Zhao, L. J. *et al.* Associations of the cerebrospinal fluid hepatocyte growth factor with
860 Alzheimer's disease pathology and cognitive function. *BMC Neurol* **21**, 387 (2021).
861 46 Noguchi, C. T., Asavaritikrai, P., Teng, R. & Jia, Y. Role of erythropoietin in the brain.
862 *Critical Reviews in Oncology/Hematology* **64**, 159-171 (2007).
863 47 Esseghir, S. *et al.* A role for glial cell–derived neurotrophic factor–induced expression by
864 inflammatory cytokines and ret/gfrα1 receptor up-regulation in breast cancer. *Cancer*
865 *research* **67**, 11732-11741 (2007).
866 48 Lin, L., Sohar, I., Lackland, H. & Lobel, P. The Human CLN2 Protein/Tripeptidyl-Peptidase
867 I Is a Serine Protease That Autoactivates at Acidic pH. *Journal of Biological Chemistry*
868 **276**, 2249-2255 (2001).

869 49 Smith, P. K., Sen, M. G., Fisher, P. R. & Annesley, S. J. Modelling of Neuronal Ceroid
870 Lipofuscinosis Type 2 in Dictyostelium discoideum Suggests That Cytopathological
871 Outcomes Result from Altered TOR Signalling. *Cells* **8**, 469 (2019).
872 50 Jonas, A. *et al.* Axonally derived matrilin-2 induces proinflammatory responses that
873 exacerbate autoimmune neuroinflammation. *Journal of Clinical Investigation* **124**, 5042-
874 5056 (2014).
875 51 Parkhurst, C. N. *et al.* Microglia promote learning-dependent synapse formation through
876 brain-derived neurotrophic factor. *Cell* **155**, 1596-1609 (2013).
877 52 Czirr, E. *et al.* Microglial complement receptor 3 regulates brain Aβ levels through secreted
878 proteolytic activity. *Journal of Experimental Medicine* **214**, 1081-1092 (2017).
879 53 Safaiyan, S. *et al.* Age-related myelin degradation burdens the clearance function of
880 microglia during aging. *Nature Neuroscience* **19**, 995-998 (2016).
881 54 Machlovi, S. I. *et al.* APOE4 confers transcriptomic and functional alterations to primary
882 mouse microglia. *Neurobiol Dis* **164**, 105615 (2022).
883 55 Tang, J. *et al.* TIMP2 ameliorates blood-brain barrier disruption in traumatic brain injury by
884 inhibiting Src-dependent VE-cadherin internalization. *The Journal of Clinical Investigation*
885 **134** (2024).
886 56 Habib, N. *et al.* Disease-associated astrocytes in Alzheimer's disease and aging. *Nature*
887 *Neuroscience* **23**, 701-706 (2020).
888 57 Ianevski, A., Giri, A. K. & Aittokallio, T. Fully-automated and ultra-fast cell-type
889 identification using specific marker combinations from single-cell transcriptomic data.
890 *Nature Communications* **13**, 1246 (2022).
891 58 Krasemann, S. *et al.* The TREM2-APOE Pathway Drives the Transcriptional Phenotype
892 of Dysfunctional Microglia in Neurodegenerative Diseases. *Immunity* **47**, 566-581.e569
893 (2017).

894 59 Escoubas, C. C. *et al.* Type-I-interferon-responsive microglia shape cortical development
895 and behavior. *Cell* **187**, 1936-1954.e1924 (2024).
896 60 Chen, X. *et al.* A brain cell atlas integrating single-cell transcriptomes across human brain
897 regions. *Nature Medicine* **30**, 2679-2691 (2024).
898 61 Masuda, T. *et al.* IRF8 is a critical transcription factor for transforming microglia into a
899 reactive phenotype. *Cell reports* **1**, 334-340 (2012).
900 62 Przanowski, P. *et al.* The signal transducers Stat1 and Stat3 and their novel target Jmjd3
901 drive the expression of inflammatory genes in microglia. *Journal of Molecular Medicine*
902 **92**, 239-254 (2014).
903 63 Pu, Z. *et al.* Regulation of Microglia-Activation-Mediated Neuroinflammation to Ameliorate
904 Ischemia-Reperfusion Injury via the STAT5-NF-κB Pathway in Ischemic Stroke. *Brain*
905 *Sciences* **12**, 1153 (2022).
906 64 Jayadev, S. *et al.* Transcription factor p53 influences microglial activation phenotype. *Glia*
907 **59**, 1402-1413 (2011).
908 65 Bido, S. *et al.* Microglia-specific *IL-10* gene delivery inhibits neuroinflammation and
909 neurodegeneration in a mouse model of Parkinson's disease. *Science Translational*
910 *Medicine* **16**, eadm8563 (2024).
911 66 Sheikh, A. M. *et al.* Aggregation of Cystatin C Changes Its Inhibitory Functions on
912 Protease Activities and Amyloid β Fibril Formation. *Int J Mol Sci* **22** (2021).
913 67 Ryan, S. K. *et al.* Microglia ferroptosis is regulated by SEC24B and contributes to
914 neurodegeneration. *Nature Neuroscience* **26**, 12-26 (2023).
915 68 Takakura, Y. *et al.* Mitochondrial protein C15ORF48 is a stress-independent inducer of
916 autophagy that regulates oxidative stress and autoimmunity. *Nature Communications* **15**,
917 953 (2024).

69 Wang, M. *et al.* Thymosin β4 reverses phenotypic polarization of glial cells and cognitive impairment via negative regulation of NF-κB signaling axis in APP/PS1 mice. *J Neuroinflammation* **18**, 146 (2021).

70 Subramanian, A. *et al.* Gene set enrichment analysis: A knowledge-based approach for interpreting genome-wide expression profiles. *Proceedings of the National Academy of Sciences* **102**, 15545-15550 (2005).

71 Jaitin, D. A. *et al.* Lipid-Associated Macrophages Control Metabolic Homeostasis in a Trem2-Dependent Manner. *Cell* **178**, 686-698.e614 (2019).

72 Frigerio, C. S. *et al.* The major risk factors for Alzheimer's disease: age, sex, and genes modulate the microglia response to Aβ plaques. *Cell reports* **27**, 1293-1306. e1296 (2019).

73 Friedman, B. A. *et al.* Diverse Brain Myeloid Expression Profiles Reveal Distinct Microglial Activation States and Aspects of Alzheimer's Disease Not Evident in Mouse Models. *Cell Reports* **22**, 832-847 (2018).

74 Heneka, M. T. *et al.* Locus ceruleus controls Alzheimer's disease pathology by modulating microglial functions through norepinephrine. *Proceedings of the National Academy of Sciences* **107**, 6058-6063 (2010).

75 Izzy, S. *et al.* Nasal anti-CD3 monoclonal antibody ameliorates traumatic brain injury, enhances microglial phagocytosis and reduces neuroinflammation via IL-10-dependent Treg–microglia crosstalk. *Nature Neuroscience* (2025).

76 Yousef, H. *et al.* Aged blood impairs hippocampal neural precursor activity and activates microglia via brain endothelial cell VCAM1. *Nature Medicine* **25**, 988-1000 (2019).

77 Hemmer, B. M., Philippi, S. M. & Castellano, J. M. Youth-associated platelet-derived chemokine reverses brain aging through neuroimmune mechanisms. *Trends in Molecular Medicine* **30**, 10-12 (2024).

78 Ayata, P. *et al.* Epigenetic regulation of brain region-specific microglia clearance activity. *Nature neuroscience* **21**, 1049-1060 (2018).

944 79 Hammond, T. R. *et al.* Single-Cell RNA Sequencing of Microglia throughout the Mouse
945 Lifespan and in the Injured Brain Reveals Complex Cell-State Changes. *Immunity* **50**, 253-
946 271.e256 (2019).
947 80 Lee, E.-J. & Kim, H.-S. The anti-inflammatory role of tissue inhibitor of metalloproteinase-
948 2 in lipopolysaccharide-stimulated microglia. *Journal of Neuroinflammation* **11**, 116
949 (2014).
950 81 Sardiello, M. *et al.* A gene network regulating lysosomal biogenesis and function. *Science*
951 **325**, 473-477 (2009).
952 82 Settembre, C. *et al.* TFEB Links Autophagy to Lysosomal Biogenesis. *Science* **332**, 1429-
953 1433 (2011).
954 83 Fadok, V. A. *et al.* Macrophages that have ingested apoptotic cells in vitro inhibit
955 proinflammatory cytokine production through autocrine/paracrine mechanisms involving
956 TGF-beta, PGE2, and PAF. *J Clin Invest* **101**, 890-898 (1998).
957 84 Podleśny-Drabiniok, A., Marcora, E. & Goate, A. M. Microglial Phagocytosis: A Disease-
958 Associated Process Emerging from Alzheimer's Disease Genetics. *Trends in*
959 *Neurosciences* **43**, 965-979 (2020).
960 85 Bohlen, C. J., Bennett, F. C. & Bennett, M. L. Isolation and Culture of Microglia. *Curr*
961 *Protoc Immunol* **125**, e70 (2019).
962 86 Podleśny-Drabiniok, A. *et al.* BHLHE40/41 regulate microglia and peripheral macrophage
963 responses associated with Alzheimer's disease and other disorders of lipid-rich tissues.
964 *Nature Communications* **15**, 2058 (2024).
965 87 Young, M. D. & Behjati, S. SoupX removes ambient RNA contamination from droplet-
966 based single-cell RNA sequencing data. *GigaScience* **9** (2020).
967 88 McGinnis, C. S., Murrow, L. M. & Gartner, Z. J. DoubletFinder: Doublet Detection in Single-
968 Cell RNA Sequencing Data Using Artificial Nearest Neighbors. *Cell Syst* **8**, 329-337.e324
969 (2019).

970 89 Andreatta, M. & Carmona, S. J. STACAS: Sub-Type Anchor Correction for Alignment in
971 Seurat to integrate single-cell RNA-seq data. *Bioinformatics* **37**, 882-884 (2021).
972 90 Miller, S. A. *et al.* LSD1 and Aberrant DNA Methylation Mediate Persistence of
973 Enteroendocrine Progenitors That Support *BRAF*-Mutant Colorectal Cancer. *Cancer*
974 *Research* **81**, 3791-3805 (2021).
975 91 Yu, G., Wang, L. G., Han, Y. & He, Q. Y. clusterProfiler: an R package for comparing
976 biological themes among gene clusters. *Omics* **16**, 284-287 (2012).
977 92 Korotkevich, G., Sukhov, V. & Sergushichev, A. Fast gene set enrichment analysis.
978 *bioRxiv*, 060012 (2019).
979 93 Kang, J. E. *et al.* Amyloid-beta dynamics are regulated by orexin and the sleep-wake cycle.
980 *Science* **326**, 1005-1007 (2009).
981

982 Figure 1

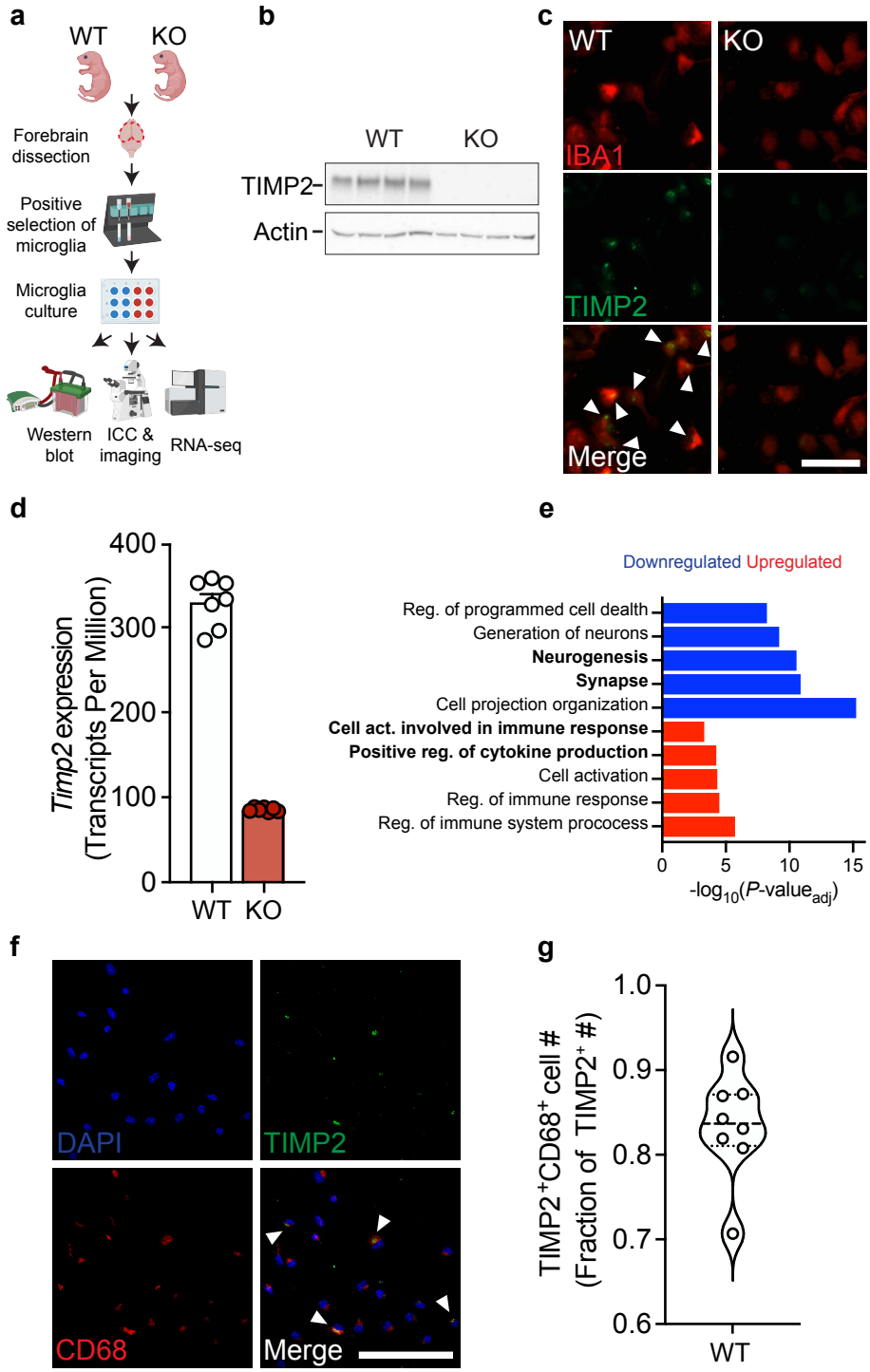
a
WT
KO
Forebrain dissection
Positive selection of microglia
Microglia culture
Western blot
ICC & imaging
RNA-seq
b
WT
KO
TIMP2
Actin
c
WT
KO
IBA1
TIMP2
Merge
d
Timp2 expression (Transcripts Per Million)
400
300
200
100
0
WT
KO
e
Downregulated
Upregulated
Reg. of programmed cell dealth
Generation of neurons
Neurogenesis
Synapse
Cell projection organization
Cell act. involved in immune response
Positive reg. of cytokine production
Cell activation
Reg. of immune response
Reg. of immune system prococess
0
5
10
15
-log10(P-value adj)
f
DAPI
TIMP2
CD68
Merge
g
TIMP2+CD68+ cell # (Fraction of TIMP2+ #)
1.0
0.9
0.8
0.7
0.6
WT

983 **Figure 1. TIMP2 is expressed in microglia and its deletion leads to phenotypes associated**
984 **with increased activation.**
985 **(a)** Schematic diagram of isolation, culturing, and assays performed on TIMP2 KO and WT
986 primary microglia. **(b)** TIMP2 immunoblotting from primary microglia lysates isolated from TIMP2
987 WT and KO littermates (N = 4 samples per genotype, comprised of 5-6 pups (P5-P8) pooled per
988 sample). **(c)** Representative images from cultures of TIMP2 KO and WT primary microglia (N = 3
989 pups (P6-P7) pooled per genotype; repeated in 2 additional experiments) stained with anti-TIMP2
990 and anti-IBA1 antibodies by ICC (scale bar = 100 μm). **(d)** Gene expression (transcript per million)
991 values for *Timp2* from bulk RNAseq experiments from TIMP2 KO and WT primary microglia (N =
992 7 samples per genotype, with each sample representing a pool of 5 pups (P6-P7); sex-matched;
993 mean ± SEM) with subsequent **(e)** over-representation analysis of GO terms ($P_{adj} < 0.05$) using
994 upregulated and downregulated DEGs in TIMP2 KO vs. WT primary microglia. **(f)** Representative
995 images from WT primary microglia cultures stained by ICC with DAPI, as well as anti-TIMP2 and
996 anti-CD68 antibodies for co-localization analyses (N = 8 mice, 5-6-month-old mice; sex-matched;
997 2 independent experiments combined; scale bar = 100 μm), with **(g)** quantification of the fraction
998 of $TIMP2^+$ cells that are $TIMP2^+CD68^+$; violin plot of median with quartiles.
999

1000 Figure 2

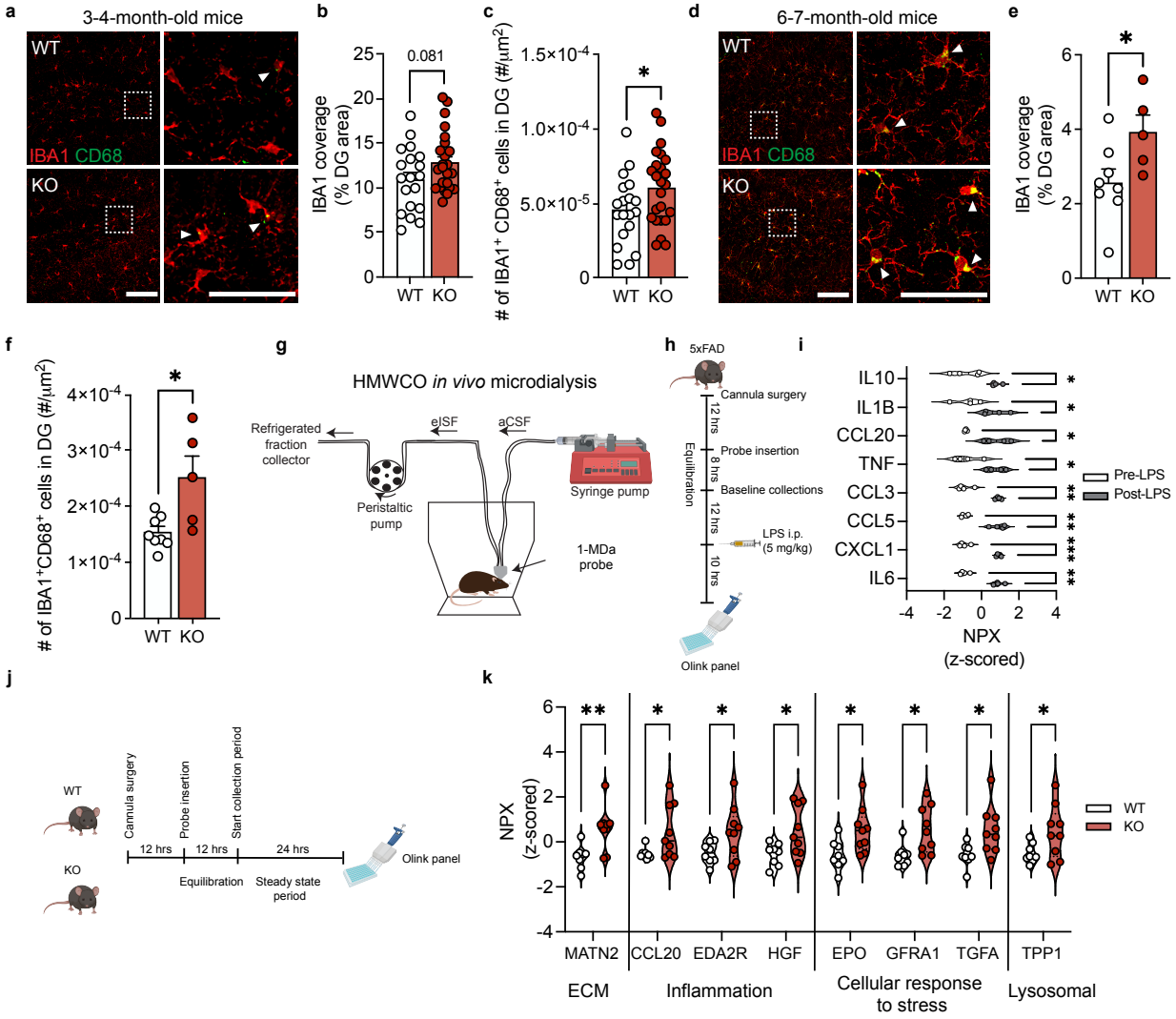

1001 **Figure 2. TIMP2 regulates microglial state and brain extracellular composition *in vivo.***
1002 **(a)** Representative confocal images of dentate gyrus (DG) of 3-4-month-old TIMP2 KO and WT
1003 mice stained with anti-IBA1 and anti-CD68 antibodies (left; scale bar = 100 μm) and magnified
1004 inset (right; scale bar = 50 μm) (N = 9-13 mice per group; sex-matched; arrowheads indicate
1005 $IBA1^+CD68^+$ cells) with corresponding **(b)** quantification of thresholded DG area covered by $IBA1^+$
1006 staining and **(c)** the number of $IBA1^+CD68^+$ cells normalized to DG area; mean ± SEM. **(d)**
1007 Representative confocal images of dentate gyrus (DG) of 6-7-month-old TIMP2 KO and WT mice
1008 stained with anti-IBA1 and anti-CD68 antibodies (left; scale bar = 100 μm) and magnified inset
1009 (right; scale bar = 50 μm) (N = 5-8 mice per group; female mice; arrowheads indicate $IBA1^+CD68^+$
1010 cells) with corresponding **(e)** quantification of thresholded DG area covered by $IBA1^+$ staining and
1011 **(f)** the number of $IBA1^+CD68^+$ cells normalized to DG area; mean ± SEM. **(g)** Schematic diagram
1012 of the high molecular-weight cut-off (HMWCO,1-MDa) *in vivo* microdialysis method to dialyze
1013 hippocampal ISF proteins and the corresponding **(h)** timeline of LPS treatment paradigm in mice
1014 undergoing microdialysis (N = 4; 6-7-month-old male 5XFAD mice) with **(i)** brain ISF protein
1015 measurements, represented as z-scored NPX values for significant proteins (paired t-test; $*P <$
1016 0.05, $**P < 0.01$, $***P < 0.001$; median with quartiles). **(j)** Timeline of HMWCO *in vivo* microdialysis
1017 experiments to evaluate steady state levels of hippocampal ISF proteins in 2-3-month-old TIMP2
1018 WT and KO mice (N = 8-9 mice per group; female mice) with corresponding **(k)** brain ISF protein
1019 measurements, represented as z-scored NPX values for significant proteins (unpaired t-test with
1020 Welch's correction; $*P < 0.05$, $**P < 0.01$; median with quartiles). Student's t test used in panels
1021 (b-c) and (e-f); $*P < 0.05$.

1022 Figure 3

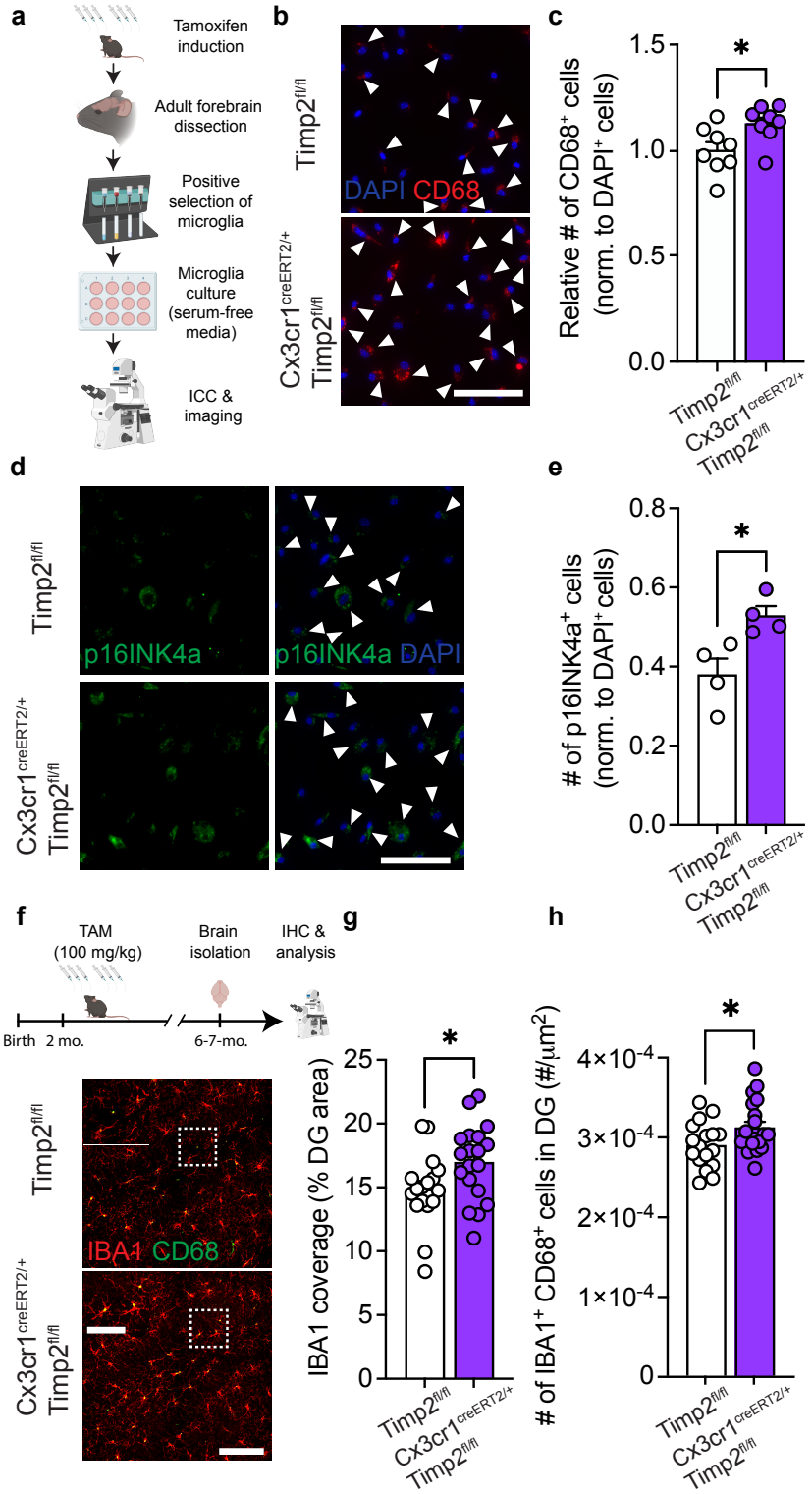

1023 **Figure 3. Removal of microglial TIMP2 increases states of activation and senescence.**
1024 **(a)** Schematic diagram of tamoxifen-inducible microglial deletion of TIMP2 in mice and
1025 subsequent isolation of adult microglia, culturing, and imaging. **(b)** Representative images from
1026 primary microglia cultures of $Timp2^{fl/fl}$ and $Cx3cr1^{CreERT2/+}$;$Timp2^{fl/fl}$ littermates stained by ICC with
1027 DAPI and anti-CD68 antibody (arrowheads indicate $CD68^+$ cells; scale bar = 100 μm) with
1028 corresponding **(c)** quantification of the number of $CD68^+$ cells normalized to total cell number
1029 ($DAPI^+$) (N = 8 mice per group; two independent experiments combined; 5-6-month-old mice; sex-
1030 matched; mean ± SEM). **(d)** Representative images from primary microglia cultures of $Timp2^{fl/fl}$
1031 and $Cx3cr1^{CreERT2/+}$;$Timp2^{fl/fl}$ littermates stained by ICC with DAPI and anti-p16INK4a antibody
1032 (arrowheads indicate $p16INK4a^+$ cells; scale bar = 100 μm) with corresponding **(e)** quantification
1033 of the number of $p16INK4a^+$ cells normalized to total number of cells ($DAPI^+$) (N = 4 mice per
1034 group, 7-month-old mice, sex-matched; mean ± SEM). **(f)** Timeline (top) of Cre induction
1035 paradigm with tamoxifen in $Timp2^{fl/fl}$ control and $Cx3cr1^{CreERT2/+}$;$Timp2^{fl/fl}$ mice and downstream
1036 processing of tissue, with representative confocal images (bottom) of DG of 6-7-month-old
1037 $Timp2^{fl/fl}$ and $Cx3cr1^{CreERT2/+}$;$Timp2^{fl/fl}$ mice stained with anti-IBA1 and anti-CD68 antibodies (scale
1038 bar = 100 μm) and magnified inset (scale bar = 50 μm) (N = 17-19 mice per group, sex-matched)
1039 with corresponding **(g)** quantification of DG area covered by anti-IBA1 staining and **(h)** the number
1040 of $IBA1^+CD68^+$ cells normalized to area. Mean ± SEM. $^*P < 0.05$; Student's t test.

Figure 4

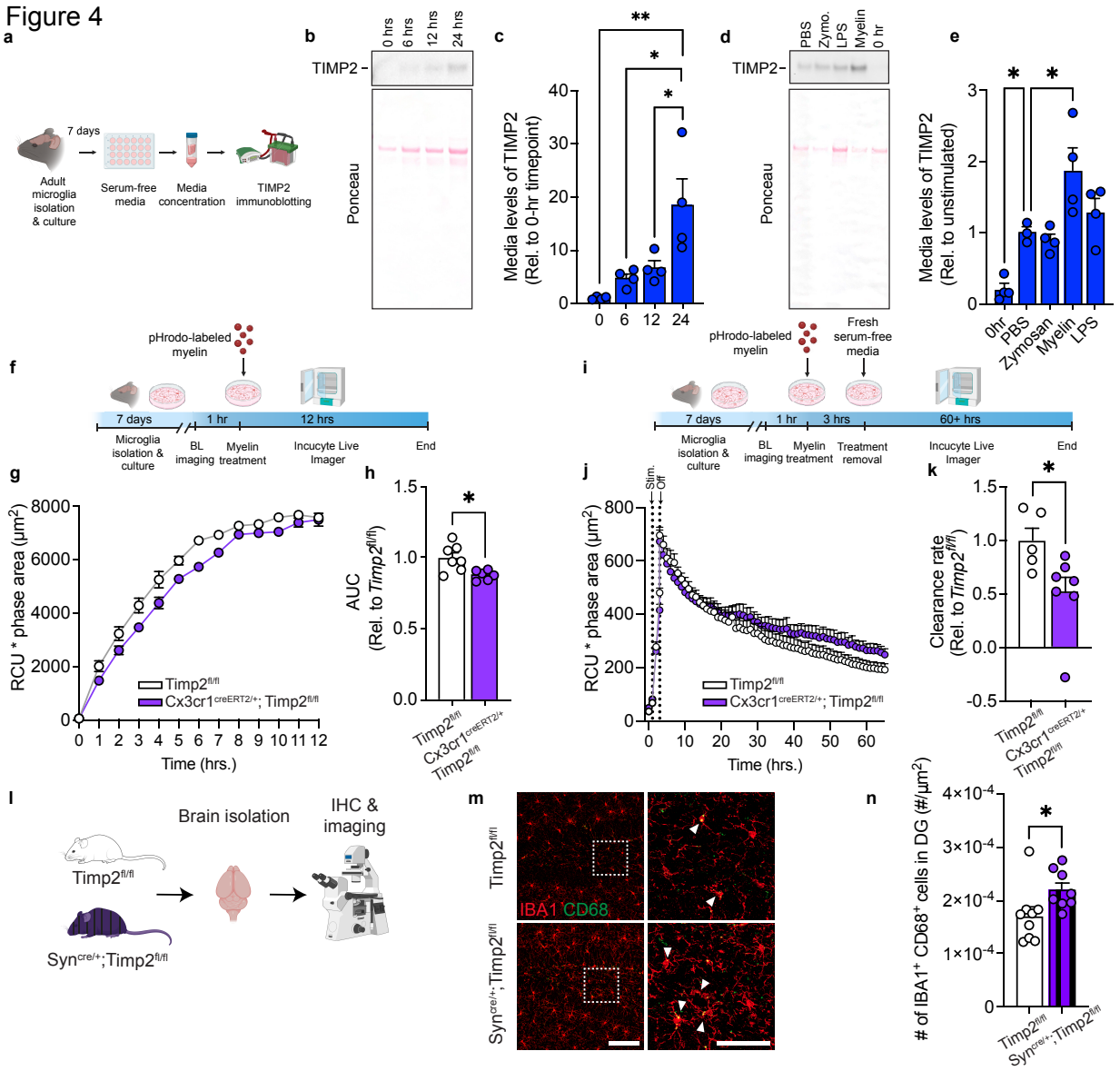

1041

1042 **Fig. 4. TIMP2 is released by microglia and alters microglial response to myelin.**
1043 **(a)** Schematic diagram showing timeline of primary microglia culturing from adult mice and media
1044 assay for TIMP2 immunoblotting experiments. **(b)** TIMP2 immunoblotting (representative) from
1045 conditioned serum-free media from primary microglia isolated from 2-month-old WT mice,
1046 including Ponceau stain (bottom), with corresponding **(c)** TIMP2 band intensity quantification (N
1047 = 4 mice per timepoint; 4 independent experiments combined, with a full timecourse for each
1048 experiment; sex-matched; mean ± SEM). **(d)** TIMP2 immunoblotting (representative) from
1049 conditioned serum-free media from primary microglia isolated from 2-month-old WT mice at
1050 baseline (0 hours with no treatment) or 12 hours following treatment with either PBS, zymosan
1051 (10 mg/mL), myelin (10 mg/mL), or LPS (100 ng/mL), with corresponding **(e)** TIMP2 band intensity
1052 quantification (N = 3-4 mice per treatment; 4 independent experiments combined, with all
1053 treatments representing an experiment; sex-matched; mean ± SEM). **(f)** Schematic diagram of
1054 treatment of adult primary microglia with pHrodo-labeled myelin and subsequent Incucyte imaging
1055 to assess uptake. (**g**) Timecourse from an experiment with total integrated density (red object
1056 mean intensity [RCU, red, *x* average phase object area (cell, μm^2)) of pHrodo-labeled myelin
1057 signal in primary microglia cultured from tamoxifen-treated 5-7-month-old Cx3cr1$^{CreERT2/+}$;Timp2$^{fl/fl}$
1058 and Timp2$^{fl/fl}$ control mice, with corresponding **(h)** uptake quantification using area under the curve
1059 (AUC; N = 6-7 mice per group; 2 independent experiments combined; sex-matched; mean ±
1060 SEM). **(i)** Schematic of experimental design to assess clearance of pHrodo-labeled myelin in
1061 Cx3cr1$^{CreERT2/+}$;Timp2$^{fl/fl}$ and Timp2$^{fl/fl}$ control mice. (**j**) Timecourse from an experiment with total
1062 integrated density (RCU [red calibrated units]) *x* average phase object area (cell, μm^2)) of pHrodo-
1063 labeled myelin signal in primary microglia cultured from 5-7-month-old tamoxifen-treated
1064 Cx3cr1$^{CreERT2/+}$;Timp2$^{fl/fl}$ and Timp2$^{fl/fl}$ control mice, with corresponding **(k)** clearance rate
1065 quantification (from slopes of regressions), represented relative to Timp2$^{fl/fl}$ control (N = 5-7 mice
1066 per group; 2 independent experiments combined; sex-matched; mean ± SEM). **(l)** Schematic

1067 diagram of neuron-specific TIMP2 deletion using *Timp2*$^{fl/fl}$ and Syn$^{Cre/+}$;*Timp2*$^{fl/fl}$ mice for confocal
1068 imaging experiments. **(m)** Representative confocal images of DG from 2-3-month-old Timp2$^{fl/fl}$
1069 and Syn$^{Cre/+}$;Timp2$^{fl/fl}$ littermates stained with anti-IBA1 and anti-CD68 antibodies (left; scale bar =
1070 100 μm) and magnified inset (right; scale bar = 50 μm; white arrowheads indicate IBA1^{+}CD68^{+}
1071 cells) with corresponding **(n)** quantification of IBA1^{+}CD68^{+} cell number normalized to DG area (N
1072 = 8-9 female mice per group; mean ± SEM). *$P < 0.05$, **$P < 0.01$; One-way ANOVA with Tukey's
1073 post hoc test (c); One-way ANOVA with Dunnett's post hoc test (e); Student's t test (h,k,n).

Figure 5

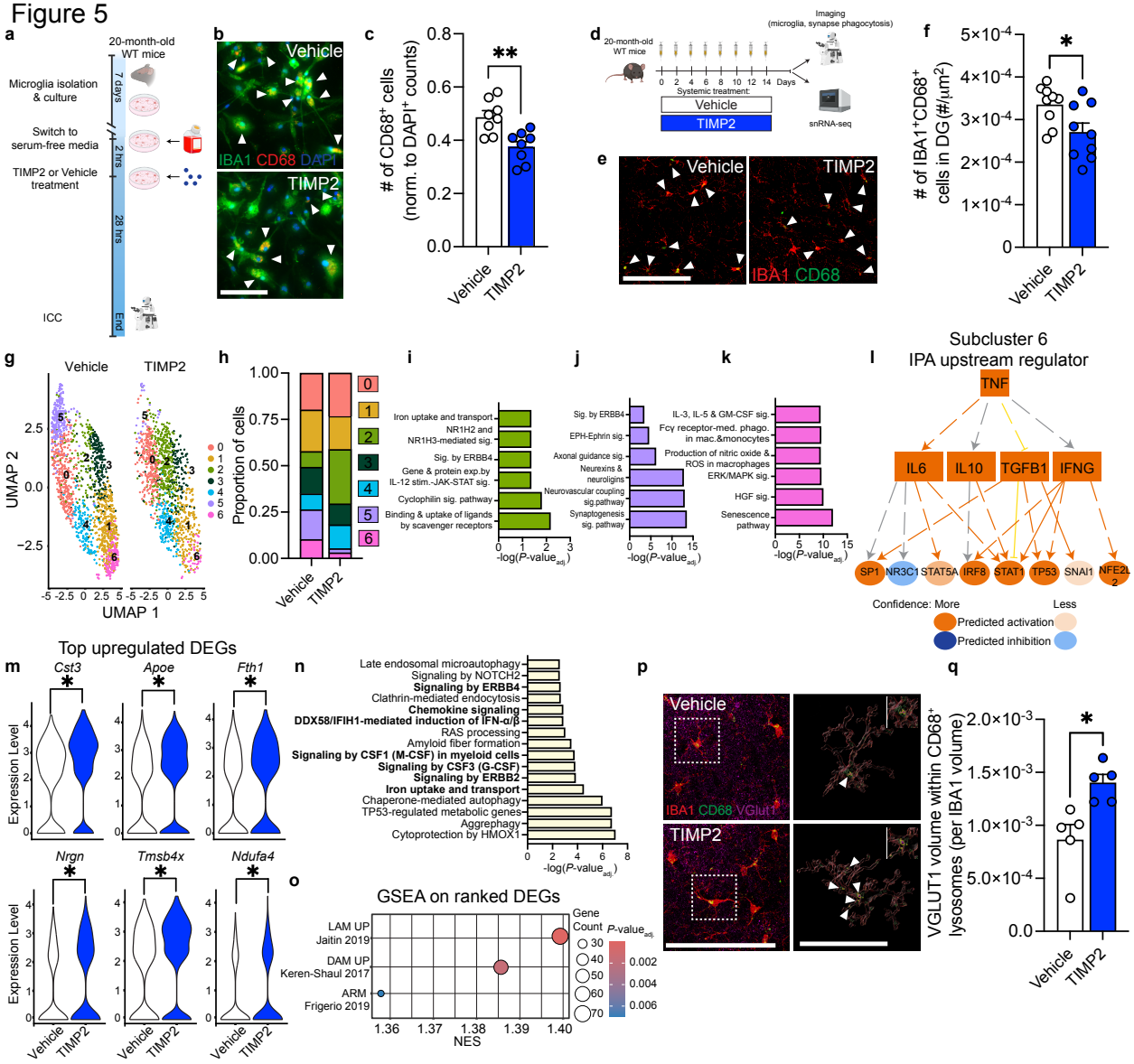

1074

1075 **Fig. 5. Youth-associated TIMP2 alters microglia in aged mice.**

1076 **(a)** Schematic of experimental timeline of microglial isolation from 20-month-old WT mice,
1077 followed by incubation with TIMP2 or vehicle. (**b)** Representative images from cultures of WT
1078 primary microglia stained with anti-IBA1 and anti-CD68 antibodies by ICC (arrowheads indicate
1079 $IBA1^{+}CD68^{+}$ cells; scale bar = 100 μm), with corresponding **(c)** quantification of the number of
1080 $CD68^{+}$ cells normalized to total cell number (N = 8 mice per treatment group, 2 independent
1081 experiments combined; sex-matched; mean ± SEM). **(d)** Schematic diagram showing paradigm
1082 of systemic treatment with recombinant TIMP2 or vehicle in 20-month-old WT mice, followed by
1083 downstream analyses. **(e)** Representative confocal images of DG from 20-month-old WT mice
1084 treated systemically with TIMP2 or vehicle, stained with anti-IBA1 and anti-CD68 antibodies (scale
1085 bar = 100 μm; white arrowheads indicate $IBA1^{+}CD68^{+}$ cells), with corresponding **(f)** quantification
1086 of number of $IBA1^{+}CD68^{+}$ cells normalized to DG area (N = 9 male mice per group; mean ± SEM).
1087 **(g)** Uniform Manifold Approximation and Projection (UMAP) plot of hippocampal microglial nuclei
1088 (2,831) isolated from 20-month-old WT mice treated systemically with vehicle or TIMP2 (N = 4
1089 male mice per group combined as 2 samples per group). **(h)** Proportion of nuclei across microglial
1090 subclusters for each treatment group with corresponding **(i)** Significant canonical pathways from
1091 IPA for marker genes significantly upregulated in subcluster 2, **(j)** subcluster 5, and **(k)** subcluster
1092 6. **(l)** IPA upstream regulator network based on subcluster 6 marker genes, with predicted
1093 relationships for target genes. **(m)** Violin plots of normalized gene expression values from
1094 selected top DEGs; $*P < 0.0001$, from DESeq2 analysis. **(n)** Significant canonical pathways from
1095 IPA on microglial DEGs ($P\text{-value}_{adj.} < 0.05$) from TIMP2-treated vs. vehicle-treated aged mice. **(o)**
1096 Dot plot from Gene Set Enrichment Analysis (GSEA) performed on ranked gene lists derived from
1097 differential expression analysis of microglia following TIMP2 treatment. Significantly enriched
1098 gene sets derived from published transcriptomic states are shown with corresponding Normalized
1099 Enrichment Score (NES), with point size representing number of overlapping genes and color
1100 indicating $P\text{-value}_{adj}$. **(p)** Representative confocal images (left) of DG from 20-month-old WT mice

1101 treated systemically with TIMP2 or vehicle, stained with anti-IBA1, anti-CD68, and anti-Vglut1
1102 antibodies (scale bar = 100 μm), with Imaris-based reconstruction (right) of insetted microglial
1103 volume (red), containing engulfed VGLUT1^{+} puncta (purple with yellow outlines indicated by white
1104 arrowheads) within microglial lysosomes (green) (scale bar = 50 μm). **(q)** Quantification of the
1105 volume of engulfed VGLUT1^{+} signal within CD68^{+} volume, normalized to microglia volume. Values
1106 represent N = 5 mice per group; mean ± SEM). *$P < 0.05$, **$P < 0.01$; Student's t test.
1107

Supplementary Figure 1

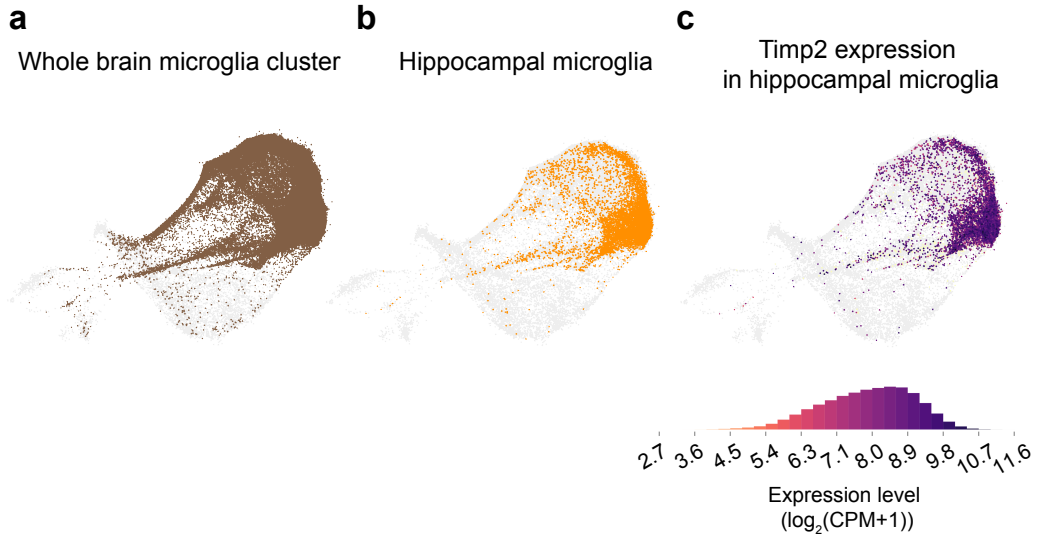

d

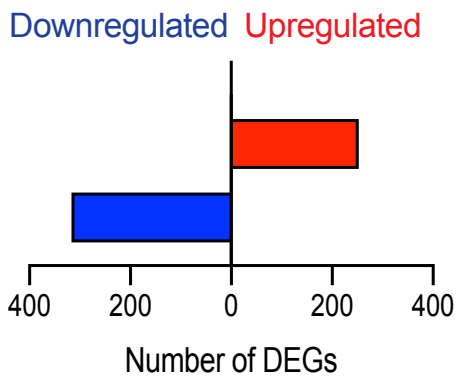

e

Canonical pathways	Predicted activation	*P*-value
Synaptogenesis signaling pathway	Inhibited	1.21E-04
Apoptosis signaling	Inhibited	9.16E-04
Synaptic long-term potentiation	Inhibited	2.49E-03
Rac signaling	Inhibited	4.59E-03
Senescence pathway	Activated	1.89E-03
Interferon gamma signaling	Activated	2.49E-03

f

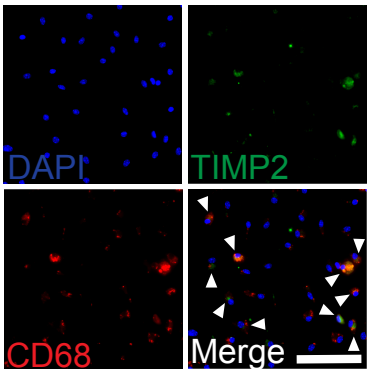

g

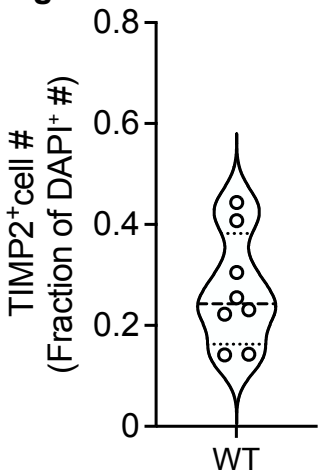

h

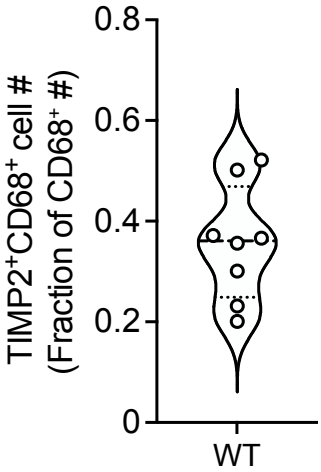

1109 **Supplementary Figure 1. Microglia express TIMP2 protein near lysosomes.**

1110 **(a)** Data from Allen Brain Cell scRNAseq and MERFISH Atlas representing whole brain microglia
1111 (brown), with subsets corresponding to **(b)** hippocampal microglia (orange), and **(c)** TIMP2
1112 expression within hippocampal microglia. **(d)** Number of upregulated and downregulated DEGs
1113 in TIMP2 KO microglia relative to WT microglia (N = 7 samples per genotype, with each sample
1114 representing a pool of 5 pups (P6-P7); sex-matched). **(e)** IPA canonical pathways based on
1115 upregulated and downregulated DEGs in TIMP2 KO and WT microglia from panel (d), with
1116 corresponding predicted inhibition or activation with *P*-values. **(f)** Representative images from WT
1117 primary microglia cultures stained by ICC with DAPI, as well as anti-TIMP2 and anti-CD68
1118 antibodies for overlap analyses (N = 8 mice, 5-6 month-old mice; sex-matched; 2 independent
1119 experiments combined; scale bar = 100 μm), with **(g)** quantification of the number of $TIMP2^+$ cells
1120 as a fraction of $DAPI^+$ cells, or **(h)** the number of $TIMP2^+CD68^+$ cells as a fraction of cells
1121 expressing CD68. Violin plots of median with quartiles.

Supplementary Figure 2

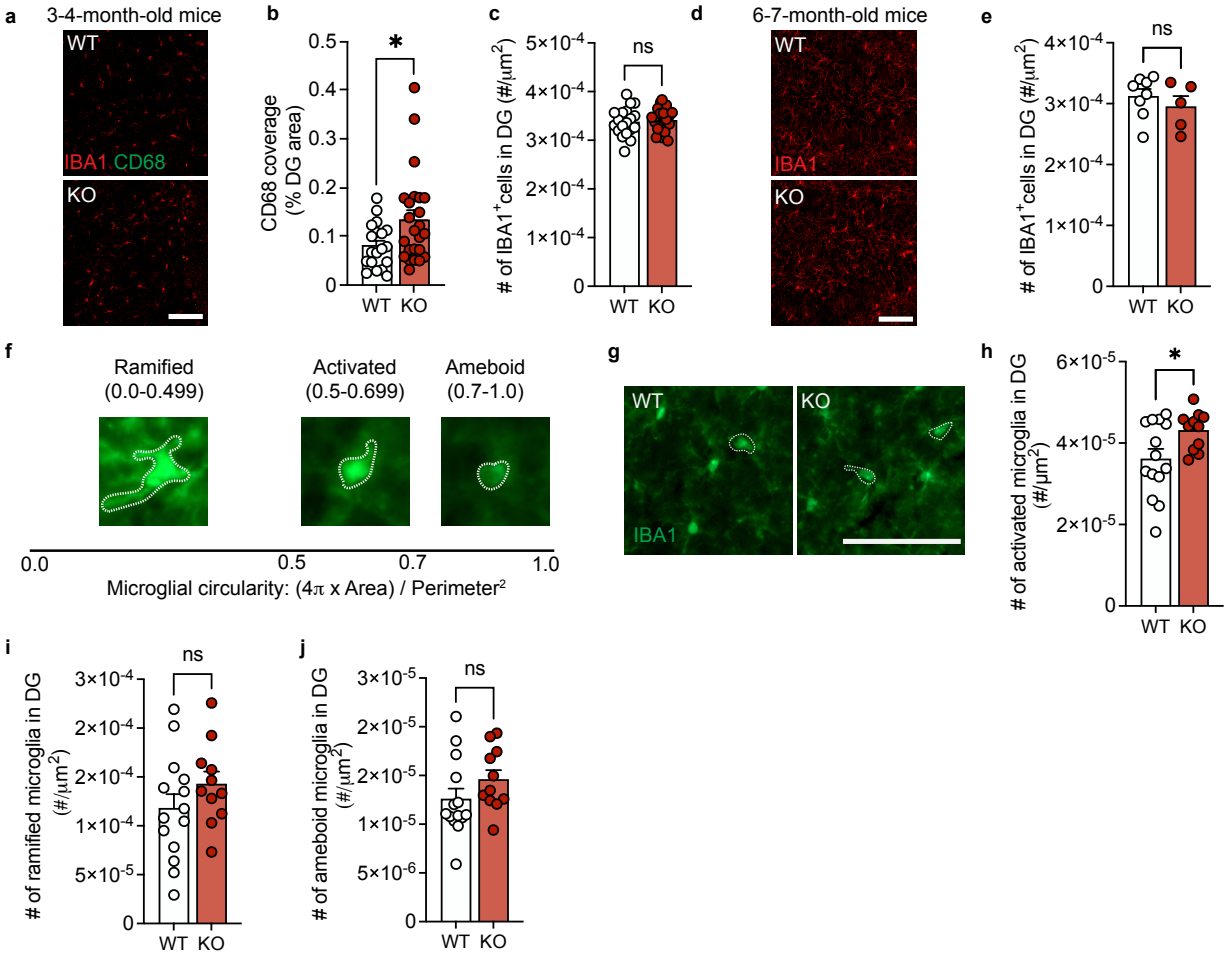

1123 **Supplementary Figure 2. TIMP2 KO mice exhibit altered state and morphology associated**
1124 **with activation.**
1125 **(a)** Representative confocal images of DG from 3-4-month-old WT and TIMP2 KO mice stained
1126 with anti-CD68 and anti-IBA1 antibodies (scale bar = 100 μm) with **(b)** quantification of
1127 thresholded DG area covered by $CD68^+$ staining and **(c)** the number of $IBA1^+$ cells normalized to
1128 DG area (N = 9-13 mice per group; sex-matched; mean ± SEM). **(d)** Representative confocal
1129 images of DG from 6-7-month-old WT and TIMP2 KO mice stained with anti-IBA1 antibody (scale
1130 bar = 100 μm) with **(e)** quantification of the number of $IBA1^+$ cells normalized to DG area (N = 5-
1131 8 mice per group; female; mean ± SEM). **(f)** Representation of morphology analysis based on
1132 microglia circularity, with representative images for each morphological state according to
1133 circularity scale. **(g)** Representative microscopy images of DG from 6-7-month-old WT and TIMP2
1134 KO mice stained with anti-IBA1 antibodies, with white dashed lines outlining microglia with
1135 "activated" morphology and corresponding (scale bar = 100 μm) **(h)** quantification of number of
1136 microglia with "activated" microglia (circularity = 0.5-0.699) per DG area. **(i)** Quantification of the
1137 number of microglia with "ramified" morphology (circularity = 0.0-0.499) per DG area, and **(j)** the
1138 number of microglia with "ameboid" microglia (circularity = 0.7-1.0) per DG area. (N = 11-14 mice
1139 per group; sex-matched; mean ± SEM). *$P < 0.05$; Student's t test; n.s., not significant.

Supplementary Figure 3

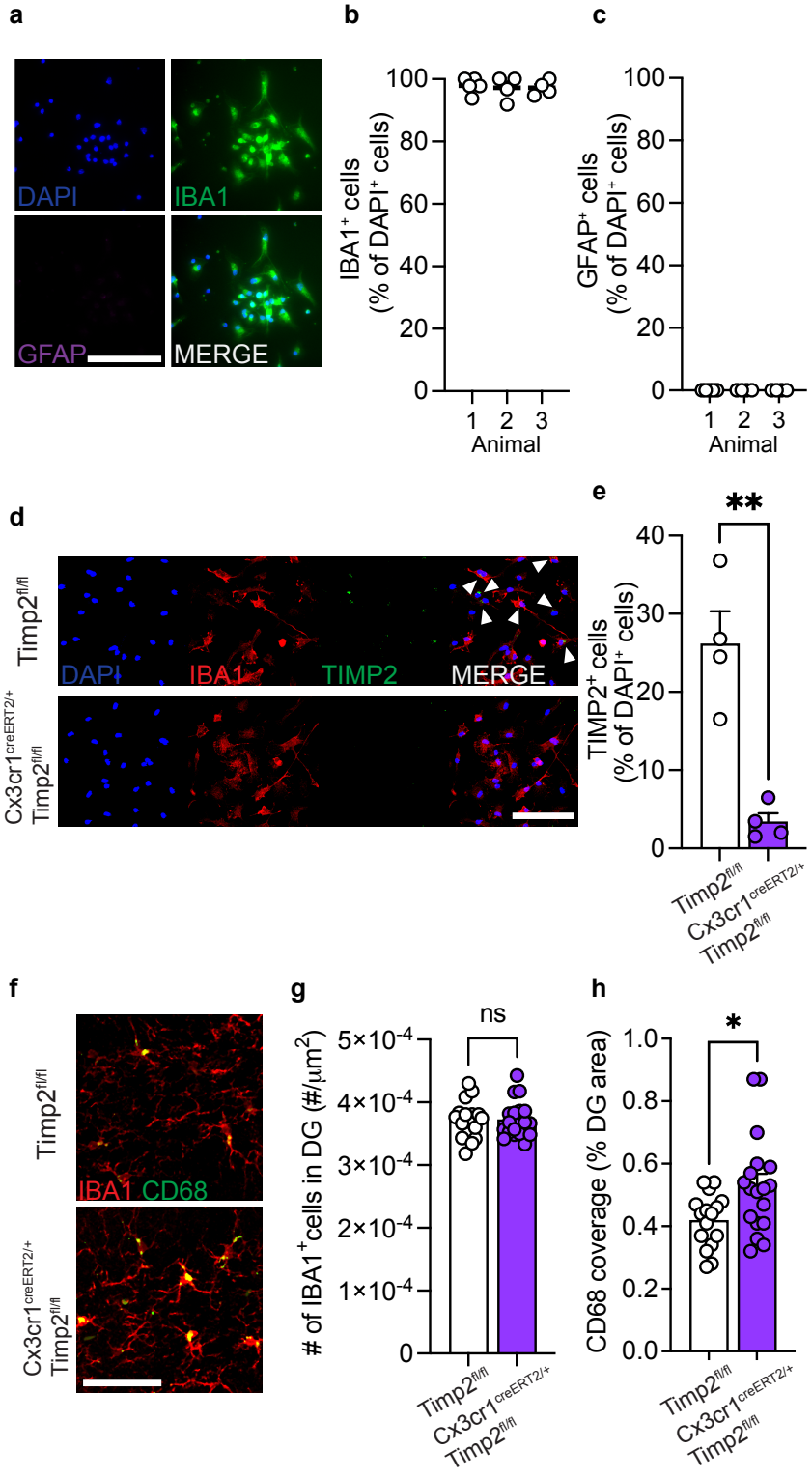

1141 **Supplementary Figure 3. Purity of primary microglia cultures and efficiency of microglia**
1142 ***Timp2* deletion**

1143 **(a)** Representative microscopy images of primary microglia cultures from WT mice stained with
1144 DAPI, anti-IBA1, and anti-GFAP antibodies (scale bar = 100 μm) with **(b)** quantification of $IBA1^+$
1145 cells as a percentage of $DAPI^+$ cells or **(c)** quantification of $GFAP^+$ cells as a percentage of $DAPI^+$
1146 cells (N = 4-5 replicates per mouse from N = 3 mice). **(d)** Representative confocal images from
1147 primary microglia cultures from 5-month-old $Timp2^{fl/fl}$ control and $Cx3cr1^{CreERT2/+}$;$Timp2^{fl/fl}$
1148 littermates stained with DAPI, anti-IBA1 antibody, and anti-TIMP2 antibody (arrowheads indicate
1149 $TIMP2^+$ microglia; N= 4 mice per group; sex-matched; scale bar = 100 μm) with **(e)** quantification
1150 of $TIMP2^+$ cells as a percentage of $DAPI^+$ cell number (mean ± SEM). **(f)** Representative confocal
1151 images of DG from 6-7-month-old $TIMP2^{fl/fl}$ control and $Cx3cr1^{CreERT2/+}$;$Timp2^{fl/fl}$ littermates stained
1152 with anti-IBA1 and anti-CD68 antibodies (N= 17-19 mice per group; sex-matched; scale bar = 50
1153 μm) with **(g)** quantification of the number of $IBA1^+$ cells per DG area and **(h)** quantification of DG
1154 area covered by $CD68^+$ staining (mean ± SEM). $^*P < 0.05$; $^{**}P < 0.01$; n.s., not significant.
1155 Student's t test.

1156 Supplementary Figure 4

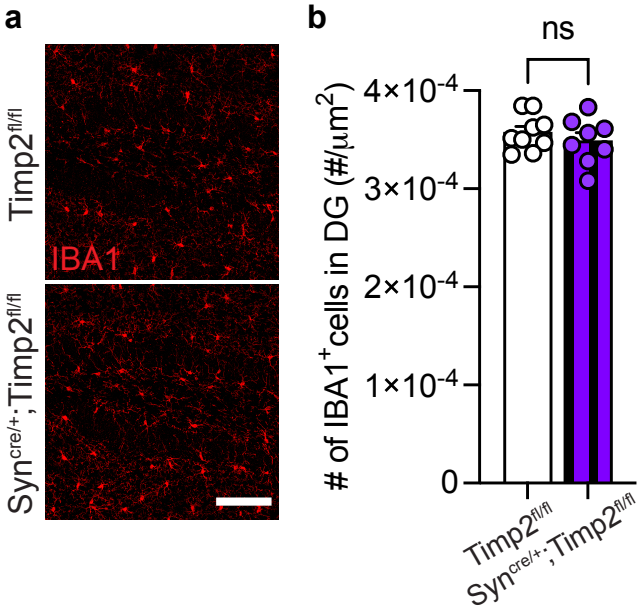

1157 **Supplementary Figure 4. Neuronal deletion of TIMP2 does not alter number of microglia in**

1158 **the dentate gyrus**

1159 **(a)** Representative confocal images of DG from *Timp2*$^{fl/fl}$ and Syn$^{Cre/+}$;*Timp2*$^{fl/fl}$ littermates stained

1160 with anti-IBA1 antibody with corresponding **(b)** quantification of the number of IBA1^{+} cells

1161 normalized to DG area (N = 8-9 mice per group, 2-3-month-old female mice; scale bar = 100 μm).

1162 mean ± SEM. ; n.s., not significant. Student's t test.

Supplementary figure 5

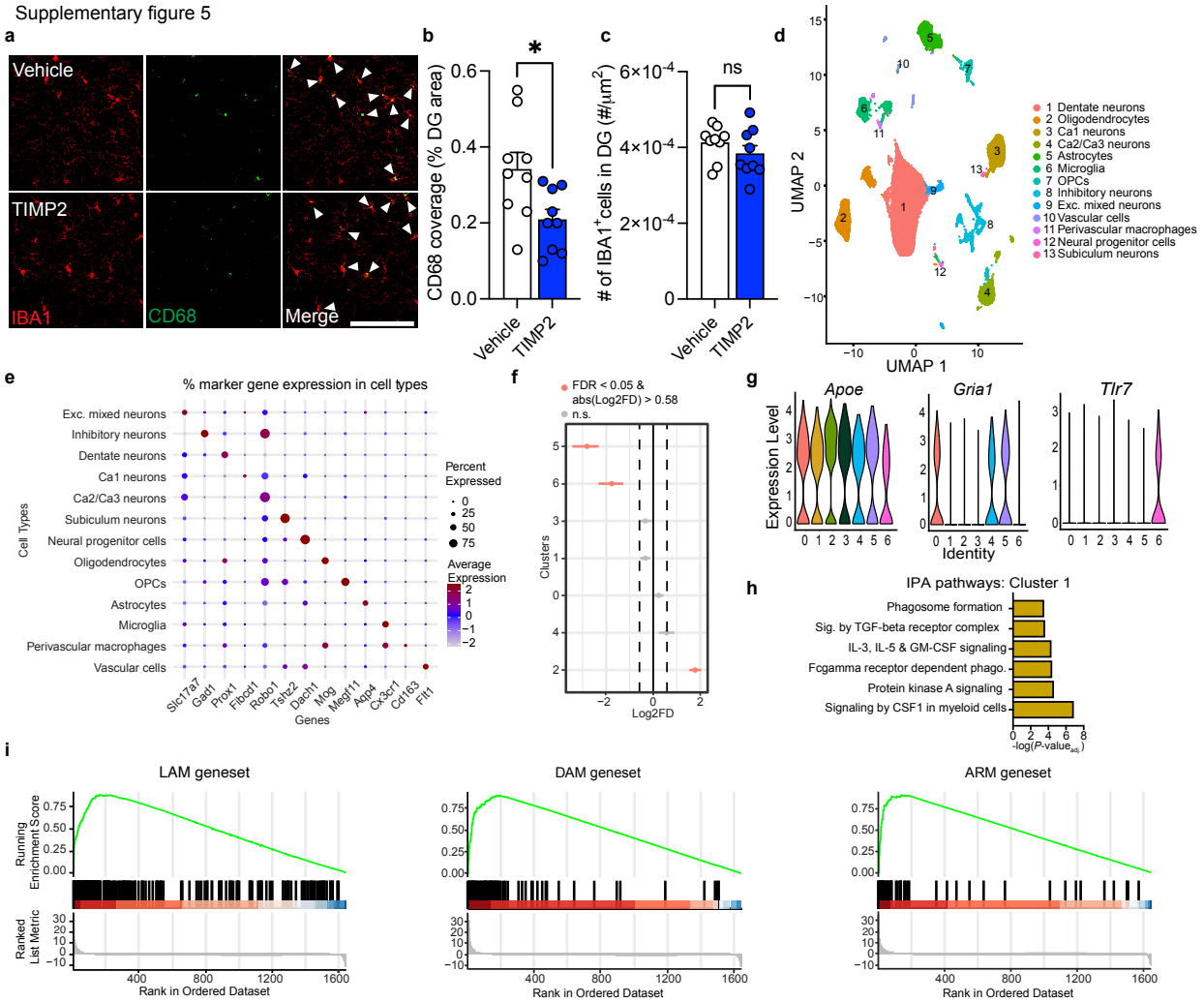

1163

1164 **Supplementary Figure 5. Systemic TIMP2 treatment in aged mice alters microglial state**
1165 **and shifts microglial subclusters.**
1166 **(a)** Representative confocal images of DG from 20-month-old WT mice treated systemically with
1167 TIMP2 or vehicle, stained with anti-IBA1 and anti-CD68 antibodies (scale bar = 100 μm; white
1168 arrowheads indicate $IBA1^{+}CD68^{+}$ cells), with corresponding **(b)** quantification of the percentage
1169 of DG area covered by $CD68^{+}$ staining and **(c)** quantification of the number of $IBA1^{+}$ cells
1170 normalized to DG area (N = 9 male mice per group; mean ± SEM). **(d)** Uniform Manifold
1171 Approximation and Projection (UMAP) plot of hippocampal nuclei isolated from 20-month-old WT
1172 mice treated systemically with vehicle or TIMP2 (N = 4 male mice per group combined as 2
1173 samples per group). **(e)** Dot plot of scaled expression of selected marker genes across annotated
1174 cell types. Dot size represents percentage of cells expressing the gene within each cell type, while
1175 color indicates the scaled average expression level of the gene across cells in the respective
1176 cluster. **(f)** Differences in cell proportions for each cluster between treatment conditions.
1177 Significant clusters are denoted in salmon (FDR < 0.05. Log_2 fold-enrichment > 0.58, relative to
1178 vehicle-treated mice). **(g)** Violin plots of selected marker genes across microglial subclusters from
1179 Fig. 5h. **(h)** Significant canonical pathways from IPA for marker genes significantly upregulated in
1180 subcluster 1. **(i)** GSEA enrichment plots for LAM, DAM, and ARM gene sets based on the ranked
1181 list of microglial genes (TIMP2 vs. vehicle). Green lines represent running enrichment score, with
1182 vertical black bars indicating the position of genes from indicated gene sets in the ranked list and
1183 gene ranking direction indicated by color bar (red = upregulated, blue = downregulated).
1184
1185